6

Normal contact of inelastic solids

6.1 Onset of plastic yield

The load at which plastic yield begins in the complex stress field of two solids in contact is related to the yield point of the softer material in a simple tension or shear test through an appropriate yield criterion. The yield of most ductile materials is usually taken to be governed either by von Mises' shear strain-energy criterion:

$$J_2 \equiv \tfrac{1}{6}\{(\sigma_1-\sigma_2)^2+(\sigma_2-\sigma_3)^2+(\sigma_3-\sigma_1)^2\} = k^2 = Y^2/3 \tag{6.1}$$

or by Tresca's maximum shear stress criterion:

$$\max\{|\sigma_1-\sigma_2|, |\sigma_2-\sigma_3|, |\sigma_3-\sigma_1|\} = 2k = Y \tag{6.2}$$

in which σ_1, σ_2 and σ_3 are the principal stresses in the state of complex stress, and k and Y denote the values of the yield stress of the material in simple shear and simple tension (or compression) respectively. Refined experiments on metal specimens, carefully controlled to be isotropic, support the von Mises criterion of yielding. However the difference in the predictions of the two criteria is not large and is hardly significant when the variance in the values of k or Y and the lack of isotropy of most materials are taken into account. It is justifiable, therefore, to employ Tresca's criterion where its algebraic simplicity makes it easier to use. A third criterion of yield, known as the maximum reduced stress criterion, is expressed:

$$\max\{|\sigma_1-\sigma|, |\sigma_2-\sigma|, |\sigma_3-\sigma|\} = k = \tfrac{2}{3}Y \tag{6.3}$$

where $\sigma = (\sigma_1+\sigma_2+\sigma_3)/3$. It may be shown from conditions of invariance that, for a stable plastic material, the Tresca criterion and the reduced stress criterion provide limits between which any acceptable yield criterion must lie. We shall see that these limits are not very wide.

(a) Two-dimensional contact of cylinders

In two-dimensional contact the condition of plane strain generally ensures that the axial stress component σ_y is the intermediate principal stress, so that by the Tresca criterion yield is governed by the maximum principal stress difference (or maximum shear stress) in the plane of cross-section, i.e. the x–z plane. Contours of principal shear stress $\tau_1 = \frac{1}{2}|\sigma_1 - \sigma_2|$ are plotted in Fig. 4.5: they are also exhibited by the photo-elastic fringes in Fig. 4.1(d). The maximum shear stress is $0.30p_0$ at a point on the z-axis at a depth $0.78a$. Substituting in the Tresca criterion (6.2) gives

$$0.60p_0 = 2k = Y$$

whence yield begins at a point $0.78a$ below the surface when the maximum contact pressure reaches the value

$$(p_0)_Y = \frac{4}{\pi} p_m = 3.3k = 1.67Y \tag{6.4}$$

The von Mises and reduced stress criteria both depend upon the third principal stress and hence upon Poisson's ratio. Taking $\nu = 0.3$, the maximum value of the left-hand side of equation (6.1) is $0.104p_0^2$ at a depth $0.70a$, and the maximum value of the left-hand side of equation (6.3) is $0.37p_0$ at a depth $0.67a$. Thus by the von Mises criterion yield begins at a point $0.70a$ below the surface when

$$(p_0)_Y = 3.1k = 1.79Y \tag{6.5}$$

and by the reduced stress criterion yield first occurs when

$$(p_0)_Y = 2.7k = 1.80Y \tag{6.6}$$

We see from the three expressions (6.4), (6.5) and (6.6) that the value of the contact pressure to initiate yield is not influenced greatly by the yield criterion used. The value given by the von Mises criterion lies between the limits set by the Tresca and reduced stress criteria.

The load for initial yield is then given by substituting the critical value of p_0 in equation (4.45) to give

$$P_Y = \frac{\pi R}{E^*} (p_0)_Y^2 \tag{6.7}$$

where the suffix Y denotes the point of first yield and $1/R = 1/R_1 + 1/R_2$.

(b) Axi-symmetric contact of solids of revolution

The maximum shear stress in the contact stress field of two solids of revolution also occurs beneath the surface on the axis of symmetry. Along this axis σ_z, σ_r and σ_θ are principal stresses and $\sigma_r = \sigma_\theta$. Their values are given by

https://doi.org/10.1017/CBO9781139171731.007 Published online by Cambridge University Press

equation (3.45). The maximum value of $|\sigma_z - \sigma_r|$, for $\nu = 0.3$, is $0.62p_0$ at a depth $0.48a$. Thus by the Tresca criterion the value of p_0 for yield is given by

$$p_0 = \tfrac{3}{2}p_m = 3.2k = 1.60Y \tag{6.8}$$

whilst by the von Mises criterion

$$p_0 = 2.8k = 1.60Y \tag{6.9}$$

The load to initiate yield is related to the maximum contact pressure by equation (4.24), which gives

$$P_Y = \frac{\pi^3 R^2}{6E^{*2}} (p_0)_Y^3 \tag{6.10}$$

It is clear from equations (6.7) and (6.10) that to carry a high load without yielding it is desirable to combine a high yield strength or hardness with a low elastic modulus.

(c) General smooth profiles

In the general case the contact area is an ellipse and the stresses are given by the equations (3.64)–(3.69). The stresses along the z-axis have been evaluated and the maximum principal stress difference is $|\sigma_y - \sigma_z|$ which lies in the plane containing the minor axis of the ellipse ($a > b$). This stress difference and hence the maximum principal shear stress τ_1 maintain an almost constant value as the eccentricity of the ellipse of contact changes from zero to unity (see Table 4.1, p. 99). Thus there is little variation in the value of the maximum contact pressure to initiate yield, given by the Tresca criterion, as the contact geometry changes from axi-symmetrical (6.8) to two-dimensional (6.4). However the point of first yield moves progressively with a change in eccentricity from a depth of $0.48a$ in the axi-symmetrical case to $0.78b$ in the two-dimensional case. Similar conclusions, lying between the results of equation (6.9) for spheres and (6.5) for cylinders, are obtained if the von Mises criterion is used.

(d) Wedge and cone

The stresses due to the elastic contact of a blunt wedge or cone pressed into contact with a flat surface were found in §5.2, where it was shown that a theoretically infinite pressure exists at the apex. It might be expected that this would inevitably cause plastic yield at the lightest load, but this is not necessarily so. Let us first consider the case of an incompressible material. During indentation by a two-dimensional frictionless wedge the tangential stress $\bar{\sigma}_x$ at the interface is equal to the normal pressure p (see eq. (2.26)). If $\nu = 0.5$ then the axial stress $\bar{\sigma}_z$ to maintain plane strain is also equal to p. Thus the stresses are hydrostatic at the contact interface. The apex is a singular point.

By considering the variation in the principal stress difference $|\sigma_x - \sigma_z|$ along the z-axis, it may be shown that this difference has a maximum but finite value of $(2E^*/\pi)\cot\alpha$ at the apex. Then by the Tresca or von Mises criteria (which are identical for $\nu = 0.5$ when stated in terms of k) yield will initiate at the apex if the wedge angle α is such that

$$\cot\alpha \geqslant \pi k/E^* \tag{6.11}$$

Similar conclusions apply to indentation by a blunt cone when $\nu = 0.5$. An infinite hydrostatic pressure is exerted at the apex of the cone but the principal stress difference $|\sigma_r - \sigma_z|$ along the z-axis is finite and has a maximum value at the apex of $E^* \cot\alpha$. In this case two principal stresses are equal, so that the Tresca and von Mises criteria are identical if expressed in terms of Y. Thus yield will initiate at the apex if the cone angle is such that

$$\cot\alpha \geqslant Y/E^* \tag{6.12}$$

For compressible materials the results obtained above are no longer true. Instead of hydrostatic pressure combined with a finite shear, the infinite elastic pressure at the apex will give rise to theoretically infinite differences in principal stresses which will cause plastic flow however small the wedge or cone angle. Nevertheless the plastic deformation arising in this way will, in fact, be very small and confined to a small region close to the apex. In the case of the wedge the lateral stress σ_y is less than σ_x and σ_z, which are equal, so that a small amount of plastic flow will take place in the y-z plane. To maintain plane strain, this flow will give rise to a compressive residual stress in the y-direction until a state of hydrostatic pressure is established. Plastic flow will then cease. Similar behaviour is to be expected in the case of the cone.

It would seem to be reasonable, therefore, to neglect the small plastic deformation which arises in this way and to retain equations (6.11) and (6.12) to express the effective initiation of yield by a wedge and a cone respectively, even for compressible materials.

Even when the limits of elastic behaviour given by the above equations have been exceeded and plastic flow has begun, the plastic zone is fully contained by the surrounding material which is still elastic. This is clearly shown in the contours of principal shear stress given by the photo-elastic fringe patterns in Figs. 4.1 and 5.2. For bodies having smooth profiles, e.g. cylinders or spheres, the plastic enclave lies beneath the surface whilst for the wedge or cone it lies adjacent to the apex. Hence the plastic strains are confined to an elastic order of magnitude and an increase in load on the cylinders or spheres or an increase in wedge or cone angle gives rise only to a slow departure of the penetration, the contact area or the pressure distribution from the values given by elastic theory. For this reason Hertz' (1882*b*) original suggestion that the *initiation* of yield due

to the impression of a hard ball could be used as a rational measure of the hardness of a material proved to be impracticable. The point of first yield is hidden beneath the surface and its effect upon measurable quantities such as mean contact pressure is virtually imperceptible. A refined attempt to detect by optical means the point of first yield during the impression of a hard ball on a flat surface has been made by Davies (1949).

We shall return to consider the growth of the plastic zone in more detail in §3, but meanwhile we shall turn to the other extreme: where the plastic deformation is so severe that elastic strains may be neglected in comparison with plastic strains. Analysis is then possible using the theory of rigid-perfectly-plastic solids.

6.2 Contact of rigid-perfectly-plastic solids

When the plastic deformation is severe so that the plastic strains are large compared with the elastic strains, the elastic deformation may be neglected. Then, provided the material does not strain-harden to a large extent, it may be idealised as a rigid-perfectly-plastic solid which flows plastically at a constant stress k in simple shear or Y in simple tension or compression. The theory of plane deformation of such materials is well developed: see, for example, Hill (1950*a*) or Ford & Alexander (1963).

A loaded body of rigid-perfectly-plastic material comprises regions in which plastic flow is taking place and regions in which, on account of the assumption of rigidity, there is no deformation. (It does not follow, however, that the stresses in the non-deforming regions are below the elastic limit.) The state of stress within the regions of flow can be represented by a *slip-line field.* The slip lines are drawn parallel to the directions of principal shearing stress at every point in the field, i.e. at 45° to the directions of principal direct stress. Thus they consist of a curvilinear net of 'α lines' and 'β lines' which are perpendicular to each other at all points. An element of such a slip-line field is shown in Fig. 6.1(*a*).

Since elastic compressibility is neglected, the principal stress acting perpendicular to the plane of deformation is given by

$$\sigma_3 = \tfrac{1}{2}(\sigma_1 + \sigma_2) \tag{6.13}$$

where σ_1 and σ_2 are the principal stresses acting in the plane of deformation. Under these conditions the Tresca and von Mises criteria of plastic flow both reduce to

$$|\sigma_1 - \sigma_2| = 2k \tag{6.14}$$

where $k = Y/2$ by Tresca or $Y/\sqrt{3}$ by von Mises. Thus the state of stress in the plastic zone comprises a variable hydrostatic stress $\frac{1}{2}(\sigma_1 + \sigma_2)$ denoted by σ,

https://doi.org/10.1017/CBO9781139171731.007 Published online by Cambridge University Press

Fig. 6.1. (*a*) Stresses acting on an element bounded by slip lines; (*b*) Mohr's circle.

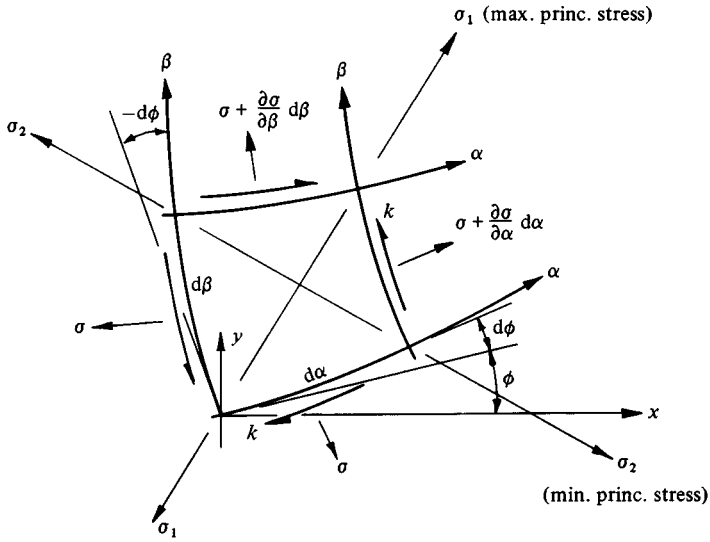

(*a*)

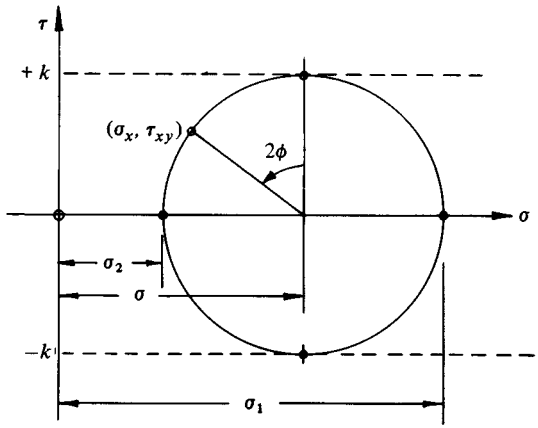

(*b*)

https://doi.org/10.1017/CBO9781139171731.007 Published online by Cambridge University Press

together with a constant simple shear k in the plane of deformation. This state of stress is represented by a Mohr's circle of constant radius k whose centre is located by the value of σ at the point in question, as shown in Fig. 6.1(*b*). The directions of the principal stresses relative to a fixed axis in the body are fixed by the directions of the slip lines. By considering the equilibrium of the element in Fig. 6.1(*a*) under the action of the direct stresses σ and the shear stress k, we obtain

$$\frac{\partial \sigma}{\partial \alpha} - 2k \frac{\partial \phi}{\partial \alpha} = 0 \tag{6.15a}$$

in the direction of an α line, and

$$\frac{\partial \sigma}{\partial \beta} + 2k \frac{\partial \phi}{\partial \beta} = 0 \tag{6.15b}$$

in the direction of a β line, which gives

$$\sigma - 2k\phi = \text{constant along an } \alpha \text{ line}\dagger \tag{6.16a}$$

$$\sigma + 2k\phi = \text{constant along a } \beta \text{ line}\dagger \tag{6.16b}$$

Thus, by starting at a point of known stress such as a free surface, equations (6.16) enable the variation in σ throughout the field to be found from the directions of the slip lines.

The constitutive relations for a plastically deforming solid relate the stresses to the small *increments* of strain. For convenience it is customary to think of the strain and displacement increments taking place in an interval of time dt and to work in terms of strain *rates* and *velocities* in place of increments of strain and displacement. The continuous deformation of the element of material shown in Fig. 6.1(*a*) consists of an extension along the direction of the maximum principal stress and a compression along the direction of the minimum principal stress. For constant volume $\dot{\epsilon}_2 = -\dot{\epsilon}_1$. There is no change in length along the direction of the slip lines, so that the deformation may be visualised as that of a 'net' in which the slip lines are inextensible strings. If a vector diagram is constructed by the velocities of particles in the deformation zone - a hodograph - the inextensibility of the slip lines requires that the 'velocity image' of a segment of a slip line is perpendicular to that line. A discontinuous mode of deformation is also possible in which an element such as that shown slides bodily relative to an adjacent element. It is clear that the line of discontinuity in particle velocity in such a deformation must coincide with a slip line.

† Some text-books take σ to be positive when *compressive*, which changes the signs in equations (6.16).

https://doi.org/10.1017/CBO9781139171731.007 Published online by Cambridge University Press

There is no progressive routine for constructing the slip-line field to solve a particular problem; it has to be found by trial. It must be self-consistent with a velocity field, and both must satisfy the boundary conditions of the problem. Finally it should be checked that the non-deforming (rigid) regions are capable of supporting the loads without violating the yield condition. When all these conditions are satisfied the slip-line field and the stresses found from it by equations (6.16) are unique, but the associated velocity field may not be.

We shall now proceed to discuss the slip-line fields associated with the rigid-plastic deformation of a wedge in contact with a plane surface. In the first instance we shall take the wedge to be appreciably harder than the flat, so that plastic deformation is confined to the flat. Secondly, we shall take the flat to be harder, so that it remains effectively rigid and crushes the apex of the wedge.

(a) Frictionless wedge indenting a rigid-plastic surface

The normal indentation of a rigid-perfectly-plastic half-space by a rigid wedge of semi-angle α is shown in Fig. 6.2(a). The material flows plastically in the two symmetrical regions lettered $ABCDE$. The material surrounding these regions, being assumed rigid, has not deformed at the current stage of indentation. The material displaced by the wedge is pushed up at the sides: for the volume to be conserved the areas of triangles AOF and FBC must be equal.

The slip-line field is shown in Fig. 6.2(a). Since the face of the wedge AB is frictionless it can sustain no shear stress. The normal pressure p_w on the wedge face is therefore a principal stress and the slip lines meet AB at 45°. Similarly the slip lines meet the free surface BC at 45°. The state of stress in the triangular region BCD is a uniform compression $2k$ acting parallel to the surface BC. It is represented by a Mohr's circle in Fig. 6.2(b). The hydrostatic component of stress in this region has the value $-k$ (shown by the centre of the circle). The state of stress in the triangular region ABE is also uniform and is represented by the other Mohr's circle. The distance between the two centres represents the difference in hydrostatic stress between the two regions, which is given by equation (6.16a) and has the value $2k\psi$, where ψ is the angle turned through by the α slip lines between the two regions. The state of stress in the fan BDE is represented by intermediate Mohr's circles whose centres are located by the inclination of the slip line at the point in question. The pressure on the wedge face is represented by point W on the circle: it has the uniform value given by

$$p_w = 2k(1 + \psi) \tag{6.17}$$

If the total normal load on the wedge is P and the projected area of contact is $2a$ per unit axial length, then the mean pressure acting normal to the original surface of the solid is given by

$$p_m = \frac{P}{2a} = p_w = 2k(1 + \psi) \tag{6.18}$$

https://doi.org/10.1017/CBO9781139171731.007 Published online by Cambridge University Press

The point B is a singular point in which the state of stress jumps from that at the free surface to that under the wedge face.

To locate the position of B and to determine the value of the angle ψ we must consider the mode of deformation. The velocity diagram (hodograph) for the right-hand deformation zone is shown in Fig. 6.2(c). The wedge is assumed to be penetrating the solid with a steady velocity V, represented by oa in the hodograph. $AEDC$, which separates the deforming region from the rigid region, is a line of discontinuity in velocity. The region ABE moves without distortion parallel to AE with the velocity oe and slides relative to the wedge face with velocity ae. The region BDC moves without distortion parallel to DC with velocity od. The velocity of the surface BC perpendicular to itself is represented by og. Now the state of stress and deformation shown in Fig. 6.2(a) should be independent of the depth of penetration: in other words geometrical similarity of the slip-line field should be maintained at all stages of the indentation. The condition of geometrical similarity controls the shape of the free surface BC. It requires that normal displacement from the origin O of any point on the

Fig. 6.2. Indentation by a rigid frictionless wedge.

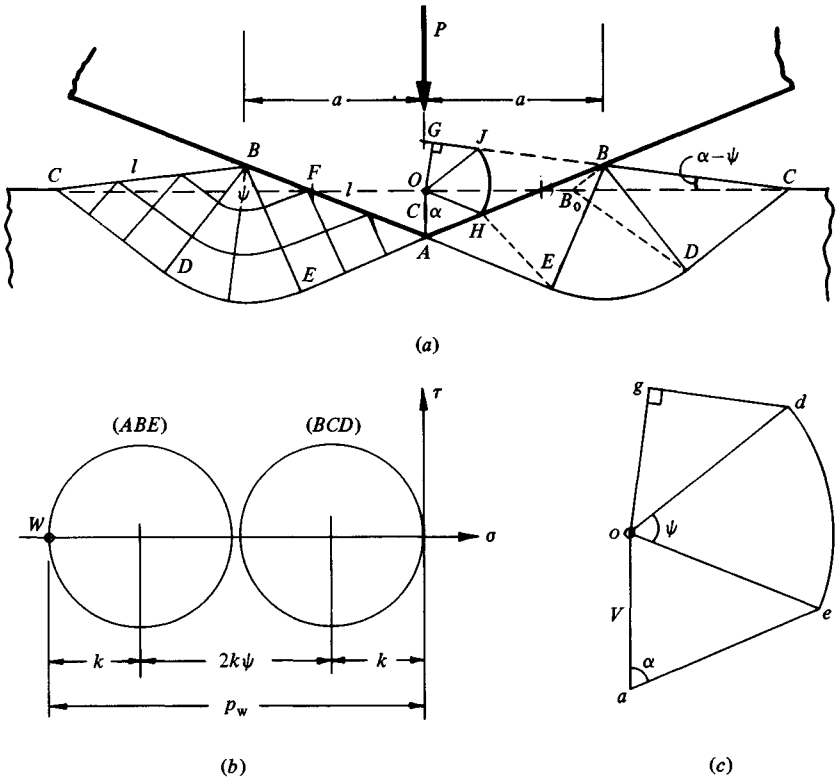

https://doi.org/10.1017/CBO9781139171731.007 Published online by Cambridge University Press

free surface BC and on the wedge face AB should grow in direct proportion to the component of velocity of that point normal to the surface. This condition may be visualised by superimposing the velocity diagram on the wedge so that o coincides with O and a with A as shown in Fig. 6.2(a). The above condition is then satisfied if the velocity image at a point on the free surface lies on the tangent to the surface at that point. In the example in Fig. 6.2, where the free surface is straight, all points on that surface have the same velocity od, so that $J(d)$ and $G(g)$ must lie on CB produced. The normal displacement of all points on BC is thus represented by OG. The angle ψ may now be found by geometry. Denoting $AB = BC = l$, the height of B above A is given by

$$l \cos \alpha = c + l \sin (\alpha - \psi) \tag{6.19}$$

The condition that G should lie on CB produced gives

$$l \cos \psi = c \sin \alpha + c \cos (\alpha - \psi) \tag{6.20}$$

Eliminating l/c from (6.19) and (6.20) gives

$$\cos (2\alpha - \psi) = \frac{\cos \psi}{1 + \sin \psi} \tag{6.21}$$

from which ψ can be found by trial for any value of α. Then substituting ψ into equation (6.18) gives the indentation pressure p_m. The variation of p_m with wedge angle α is shown by the curve marked 'frictionless' in Fig. 6.7.

Returning to examine the mode of deformation more closely, we observe that material particles originally lying along the internal line OA are displaced to lie along the wedge face in the segment AH. Thus the nose of the wedge acts like a cutting tool. Material lying within the triangle OAE has been displaced to HAE. Particles lying within the triangle BDC have moved in the direction od parallel to DC. Thus B originally lay on the surface at B_0 where B_0B is parallel to DC, and material in the deformed region BDC originally lay in the region B_0DC. Material originally in the region OB_0DE has undergone a more complex deformation governed by the fan of slip lines BDE. The segment of the original surface OB_0 is folded into contact with the wedge face along BH. The distortion of a square grid calculated from the hodograph is shown in Fig. 6.3(a). Details of the method of calculation are given in the original paper by Hill *et al.* (1947).

(b) Influence of friction on wedge indentation

Friction between the face of the wedge and the indented material influences the mode of deformation significantly. The relative motion of the material up the face of the wedge now introduces an opposing shear stress $\tau_w = \mu p_w$ so that the slip lines intersect the face of the wedge at an angle $ABE = \lambda$ which is less than 45°. The modified slip-line field, and Mohr's circle

https://doi.org/10.1017/CBO9781139171731.007 Published online by Cambridge University Press

for the stress at the wedge face, are shown in Fig. 6.4. The pressure on the wedge face is now given by

$$p_w = k(1 + 2\psi + \sin 2\lambda) \tag{6.22}$$

and the shear stress is

$$\tau_w = k \cos 2\lambda \tag{6.23}$$

hence λ is related to the coefficient of friction by

$$\cos 2\lambda = \mu(1 + 2\psi + \sin 2\lambda) \tag{6.24}$$

Equilibrium of the wedge gives the indentation pressure

$$p_m = \frac{P}{2a} = p_w(1 + \mu \cot \alpha) \tag{6.25}$$

Fig. 6.3. Deformation by a blunt wedge: (*a*) frictionless; (*b*) no slip.

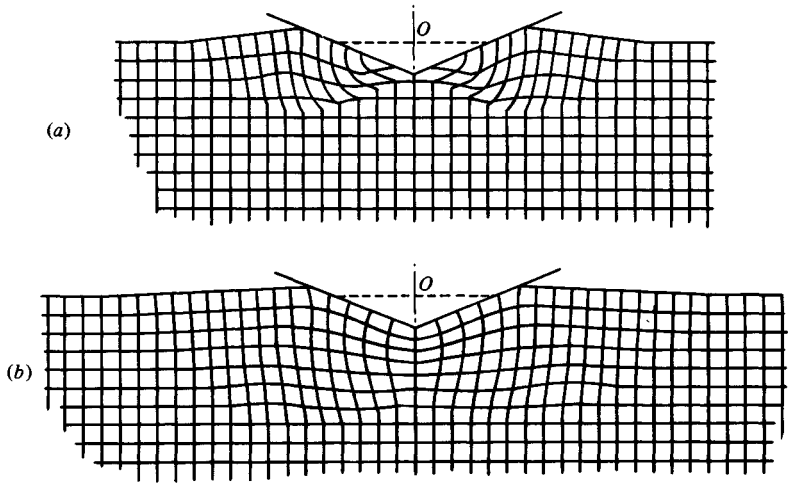

Fig. 6.4. Indentation by a rough wedge with slip at the interface.

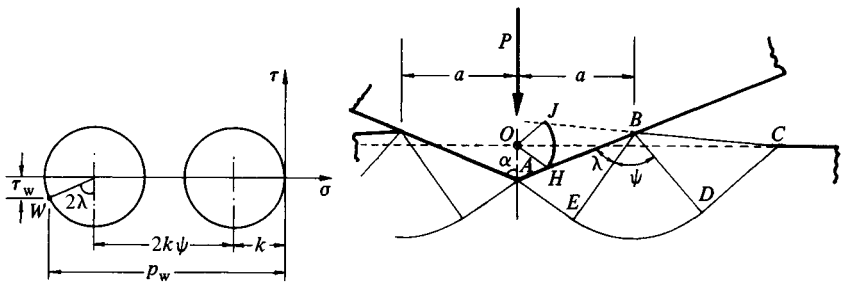

https://doi.org/10.1017/CBO9781139171731.007 Published online by Cambridge University Press

When the hodograph is superimposed on the diagram of the wedge, as before, the condition of similarity requires that J should again lie on the line of the free surface BC produced. The determination of the angles ψ and λ for given values of α and μ must be carried out by a process of trial. Such calculations were made by Grunsweig, Longman & Petch (1954) and the results are plotted in Fig. 6.7.

We note that friction causes the point H to move towards the apex of the wedge which reduces the cutting action. With increasing friction a limit is reached when slip at the wedge face ceases: the surface of the solid adheres to the wedge and shear takes place in the body of the material. For a wedge of semi-angle less than 45°, the limiting slip-line field is shown in Fig. 6.5. A slip line coincides with the wedge face and concentrated shearing takes place just within the material at a shear stress $\tau_w = k$. The critical value of μ and the corresponding pressures are found by putting $\lambda = 0$ in equations (6.24), (6.22) and (6.25).

With a blunt wedge ($\alpha > 45°$) this solution is incorrect since the slip lines at the apex cannot meet at an angle less than 90°. In this case a cap of undeforming material adheres to the wedge and shear takes place on slip line BE, as shown in Fig. 6.6. The stress state along the slip line BE is indicated by point S on the Mohr's circle. Equilibrium of the cap of metal ABE results in the stresses on the face of the wedge being represented by W, i.e. the normal stress is $k(1 + 2\psi - \cos 2\alpha)$ and the shear stress is $k \sin 2\alpha$. Hence for the cap to adhere to the wedge

$$\mu \geqslant \frac{\sin 2\alpha}{1 + 2\psi - \cos 2\alpha} \tag{6.26}$$

whereupon the indentation pressure is given by

$$p_m = \frac{P}{2a} = 2k(1 + \psi) \tag{6.27}$$

Fig. 6.5. Indentation by a sharp wedge with no slip.

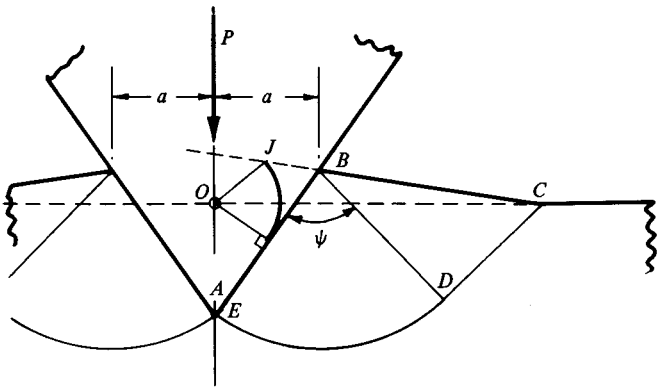

https://doi.org/10.1017/CBO9781139171731.007 Published online by Cambridge University Press

As before, ψ is determined from the hodograph and the condition of geometrical similarity. Values have been found by Haddow (1967) and are shown in Fig. 6.7.

The distortion of a square grid in the mode of deformation involving a built-up nose on the wedge has been constructed and is shown in Fig. 6.3(*b*) for direct comparison with the frictionless mode. The difference is striking. Deformation occurs beneath the apex of the wedge and the displacements of grid points from their undeformed positions are approximately radial from *O*.

The influence of strain hardening on the slip-line field for an indenting wedge has been investigated by Bhasin *et al.* (1980).

(c) Crushing of a plastic wedge by a rigid flat

If the wedge is appreciably softer than the flat surface the wedge will deform plastically and the flat will remain rigid. The slip-line field suggested by Hill (1950*a*) for frictionless contact between the wedge and the plane is shown in Fig. 6.8(*a*). *AEDC* is a line of velocity discontinuity. The triangular region *ABE* slides outwards relative to the face of the flat and, in the absence of fric-tin, the slip lines meet the interface at 45°. The pressure on the interface is uniform and given by

$$p_m = \frac{P}{2a} = 2k(1 + \psi) \tag{6.28}$$

where the angle ψ is determined by the condition of geometrical similarity, that *J* should lie on *CB* produced.

Fig. 6.6. Indentation by a blunt wedge with no slip.

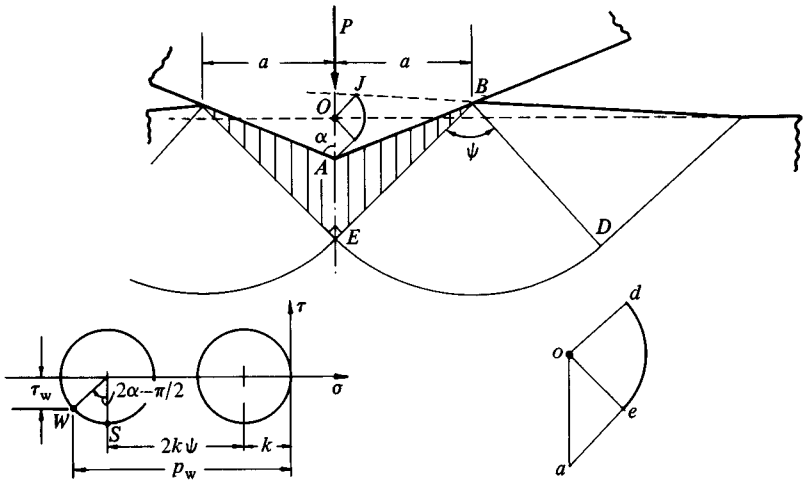

https://doi.org/10.1017/CBO9781139171731.007 Published online by Cambridge University Press

An alternative mode of deformation and associated slip-line field is shown in Fig. 6.8(*b*). The triangular region *ABE* adheres to the flat and moves vertically with it and there is intense shear on the slip line *BE*. The pressure on the interface is still given by equation (6.28) but, in this case, the angle is slightly larger than before so that the pressure required to produce this mode of deformation is higher, as shown in Fig. 6.9. The difference in pressure is due to the difference in inclination on the surface *BC* of the shoulders.

For an ideally frictionless flat it is to be presumed that the deformation would follow the pattern in Fig. 6.8(*a*) since this requires the lowest pressure to cause deformation.† Friction at the interface will oppose the sliding motion and cause the slip lines to meet the surface at *B* and *B'* at less than 45°. This would result in an unacceptable state of stress at *A* unless a cap of undeforming material adheres to the contacting flat in the vicinity of *A*, in the manner found when a rectangular block is compressed between two flat rigid plates (see Ford & Alexander, 1963). The slip-line field and the profile of the free surfaces *BC*

† Asymmetrical modes of deformation are also possible but, since they require higher pressures than the symmetrical mode, they will not be considered.

Fig. 6.7. Mean contact pressure for a rigid wedge indenting a rigid-perfectly-plastic half-space.

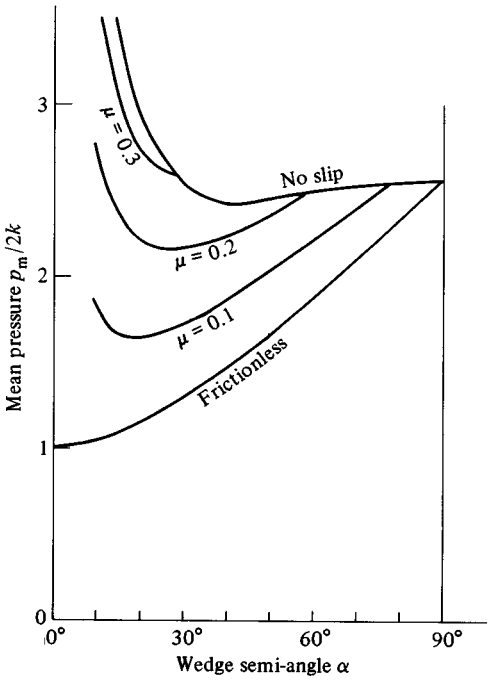

https://doi.org/10.1017/CBO9781139171731.007 Published online by Cambridge University Press

Fig. 6.8. Crushing of a plastic wedge by a rigid flat: (*a*) frictionless; (*b*) no slip.

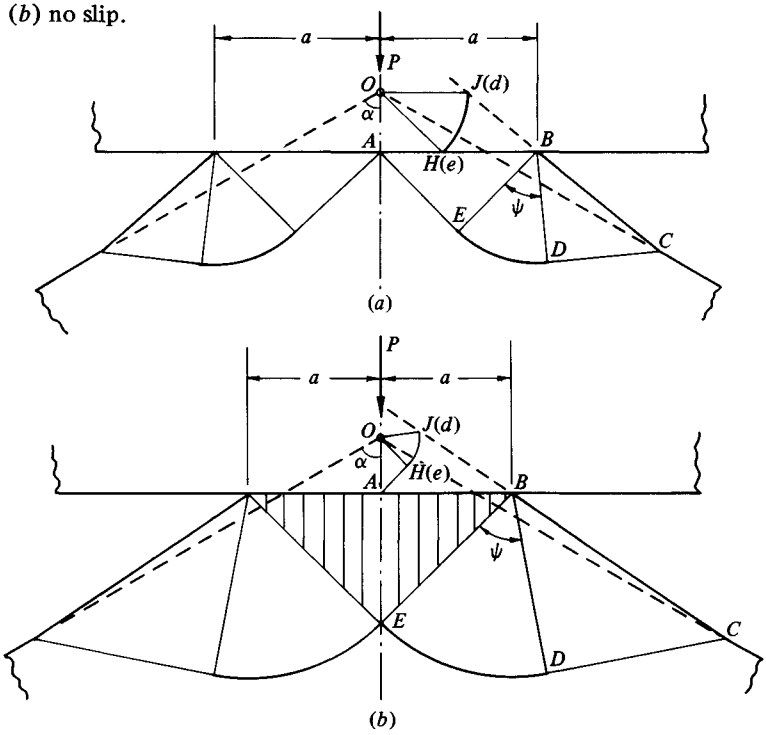

Fig. 6.9. Contact pressure on a flat crushing a plastic wedge.

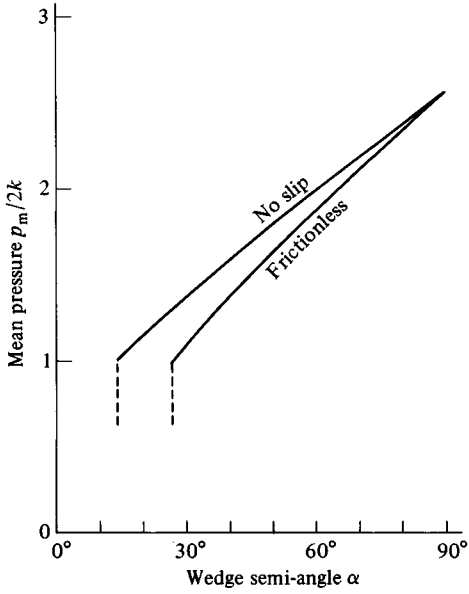

https://doi.org/10.1017/CBO9781139171731.007 Published online by Cambridge University Press

will then be curved. This problem has not yet been solved quantitatively, so that it is not possible to say exactly how much interfacial friction is necessary to eliminate sliding and ensure that the adhesive mode of Fig. 6.8(*b*) is obtained.† This is not a serious shortcoming, however, since the difference in indentation pressure between the frictionless and adhesive modes is not large. It is somewhat paradoxical that although friction is necessary to ensure that the adhesive mode takes place, when it does so no friction forces are transmitted at the interface.

The paradox arises (*a*) through the neglect of *elastic* deformation which will influence the frictional conditions at the interface in the 'adhesive' mode and (*b*) through the assumption of perfect plasticity which leads in some cases to a lack of uniqueness in the mode of deformation. Strain hardening, which is a feature of real materials, will favour the mode of deformation in which the plastic strains are least and are most uniformly distributed through the deforming region.

The solutions given in Fig. 6.8 cease to apply when the angle ψ vanishes. In the limit ($\alpha = 26.6°$ and $\alpha = 14°$ respectively) the sides of the shoulders of displaced material are parallel and the deforming region of the wedge is in simple compression.

If the wedge and the flat are of comparable hardness both will deform. This state of affairs has been examined by Johnson *et al.* (1964) who have determined the limiting values of the yield stress ratio for the deformation to be restricted to either the wedge or the flat.

(d) Conical indenters

Problems of axi-symmetrical plastic flow cannot, in general, be solved by the method of characteristics (slip lines) as in plane strain. However Shield (1955) has shown that, in certain cases, for material which flows plastically according to the Tresca criterion, a slip-line field can be constructed which specifies the state of stress. Such a field must be consistent with an associated velocity field of axi-symmetrical deformation. As an example Shield found the stresses in a rigid-plastic semi-infinite solid under the action of a frictionless, flat-ended, cylindrical punch. Following Shield's method, Lockett (1963) was able to construct the fields due to a rigid frictionless cone penetrating a flat

† An estimate of the *average* friction force necessary to produce the adhesive mode may be obtained by applying the principle of virtual work to the frictionless mode with friction forces introduced at the interface. The calculation gives the critical coefficient of friction as

$$\mu_c \approx 1 - (p_m)_s/(p_m)_a$$

where $(p_m)_s$ and $(p_m)_a$ are the values of p_m in the frictionless and adhesive modes respectively. It is apparent from Fig. 6.9 that the value of μ_c is generally small.

https://doi.org/10.1017/CBO9781139171731.007 Published online by Cambridge University Press

surface, provided the semi-cone-angle α exceeded 52.5°. The slip-line field is similar to that for a two-dimensional wedge shown in Fig. 6.8, but the slip lines and the profile of the deformed surface are no longer straight. The pressure on the surface of the cone is not uniform but rises to a peak at the apex. The limiting case, where $\alpha = 90°$, corresponds to the cylindrical punch studied by Shield. The pressure distributions and the mean indentation pressures are shown in Fig. 6.10. The mean pressure is slightly higher than that of a frictionless wedge of the same angle.

Indentation by a cylindrical punch in which the material does not slip relative to the flat face of the punch has been analysed by Eason & Shield (1960). A cone of undeforming material adheres to the surface of the punch. The mean contact pressure is $6.05k$ compared with $5.69k$ for a frictionless punch. Strictly speaking the distribution of stress in the cone of material adhering to the punch is indeterminate, but an indication may be obtained by continuing the slip-line field into this region, which results in the pressure distribution on the punch face shown by the broken line in Fig. 6.10. From the ratio of shear stress to normal pressure it transpires that a coefficient of friction >0.14 is required to prevent slip.

Fig. 6.10. Indentation of a rigid-plastic half-space by a rigid cone. Solid line – smooth, Lockett (1963); broken line – adhesive, Eason & Shield (1960).

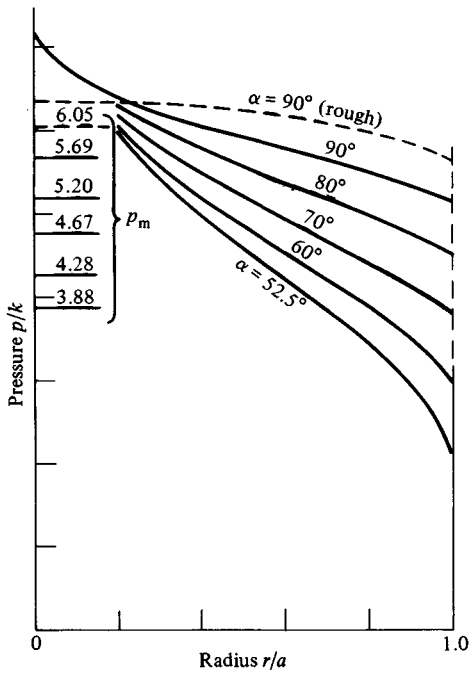

https://doi.org/10.1017/CBO9781139171731.007 Published online by Cambridge University Press

(e) Curved indenters

When an indenter having a convex profile is pressed into a surface geometrical similarity is not maintained. The intensity of strain increases with increasing penetration. The slip-line field is curvilinear and difficulties of analysis arise with the changing shape of the free surface. By assuming that the free surface remains flat, Ishlinsky (1944) constructed a field for the indentation of a rigid-plastic half-space by a rigid frictionless sphere.† In an indentation for which the ratio of contact radius to sphere radius $a/R = 0.376$, the mean indentation pressure was found to be $5.32k$.

An exact solution has been found by Richmond *et al.* (1974) for indentation of a perfectly-plastic half-space by a rigid sphere with no slip at the interface. The mean contact pressure is found to be almost independent of the penetration, varying from $6.04k$ when $a/R = 0.07$ to $5.91k$ when $a/R = 0.30$ (cf. $6.05k$ for the flat punch). This result is not surprising when it is remembered that the indenter is covered by a nose of undeforming material; the profile of the indenter can then only influence the contact pressure through small changes in the profile of the free surface outside the contact.

In the slip-line fields considered in this section the boundary which separates the plastically deforming region from the region below it should not be confused with the elastic-plastic boundary which exists in any real material having some elasticity. Rigid-plastic theory is not able to locate the elastic-plastic boundary, but a rough estimate of its position in a plane-strain indentation may be obtained from the elastic stress distribution under a uniform pressure acting on a half-space given by equations (2.30) *et seq.* Contours of constant principal shear stress τ_1 are circles through the edges of the contact as shown in Fig. 2.7(*a*). Taking the indentation pressure for a blunt wedge to be $5.1k$, τ_1 will have the value k along the circular contour of radius $1.6a$. If this circle is taken as a first approximation to the elastic-plastic boundary, the plastic zone extends to a depth of $2.9a$ beneath the point of first contact. This is well below the boundaries of the deforming region shown in Figs. 6.2, 6.3, 6.4 or 6.5. Another simple approach to finding the position of the elastic-plastic boundary is given in §3.

A method for extending the slip-line field into the rigid region has been described by Bishop (1953). He has extended the field around a two-dimensional flat-ended punch (wedge angle $\alpha = 90°$) until a boundary of zero stress is reached. Provided these boundaries lie wholly within the actual free surfaces of the solid body which is being indented, it can be concluded that the rigid

† It has been shown subsequently that the slip-line field proposed by Ishlinsky is not compatible with the associated velocity field, since there are some regions in which the plastic work is non-positive. His result must be regarded, therefore, as approximate. No exact solutions have been found for *frictionless* curved indenters.

https://doi.org/10.1017/CBO9781139171731.007 Published online by Cambridge University Press

region can support the stresses given by the slip-line field in the deforming region without plastic failure occurring elsewhere. From this construction the minimum dimensions of a rectangular block can be found to ensure that the indentation is not influenced by the size of the block. The minimum depth is $8.8a$ and the minimum width from the centre-line of the impression to the side of the block is $8.7a$, where a is the half-width of the punch. Since the flat punch is the most severe case, a block of the above dimensions would contain the indentation made by any other profile. For further discussion of this question see Hill (1950*b*).

An extension of the field under a flat-ended cylindrical punch by Shield (1955) shows that the indented solid should have a minimum depth of $3.4a$ and a minimum radius from the axis of the indenter of $3.2a$.

Strain hardening, discussed in more detail in §3, has the effect of pushing the elastic-plastic boundary, where the yield stress is lower than in the more severely strained region close to the indenter, further into the solid than perfectly plastic theory would predict. Thus a block of strain-hardening material should be somewhat larger than the critical dimensions given above to ensure that the impression is not influenced by the size of the block (see experiments by Dugdale, 1953, 1954).

6.3 Elastic-plastic indentation

The elasticity of real materials plays an important part in the plastic indentation process. When the yield point is first exceeded the plastic zone is small and fully contained by material which remains elastic so that the plastic strains are of the same order of magnitude as the surrounding elastic strains. In these circumstances the material displaced by the indenter is accommodated by an elastic expansion of the surrounding solid. As the indentation becomes more severe, either by increasing the load on a curved indenter or by using a more acute-angled wedge or cone, an increasing pressure is required beneath the indenter to produce the necessary expansion. Eventually the plastic zone breaks out to the free surface and the displaced material is free to escape by plastic flow to the sides of the indenter. This is the 'uncontained' mode of deformation analysed by the theory of rigid-plastic solids in the previous section. We would expect the plastic zone to break out to the surface and the uncontained mode to become possible when the pressure beneath the indenter reaches the value given by rigid-plastic theory. From the results of the previous section we can write this pressure:

$$p_{\mathrm{m}} = cY \tag{6.29}$$

where c has a value about 3.0 depending on the geometry of the indenter and friction at the interface. From the results of §6.1, first yield is also given by

https://doi.org/10.1017/CBO9781139171731.007 Published online by Cambridge University Press

equation (6.29), where the constant c has a value about unity. There is a transitional range of contact pressures, lying between Y and $3Y$, where the plastic flow is contained by elastic material and the mode of deformation is one of roughly radial expansion. The three ranges of loading: purely elastic, elastic-plastic (contained) and fully plastic (uncontained) are a common feature of most engineering structures.

The deformation of an elastic-perfectly-plastic material is governed by the stress–strain relations of Reuss (see Hill, 1950*a* or Ford & Alexander, 1963). In principle the contact stresses due to an elastic-plastic indentation in which the strains remain small can be calculated. In practice this is very difficult because the shape and size of the elastic-plastic boundary is not known *a priori*. The technique whereby the solid continuum is replaced by a mesh of 'finite elements' shows promise, but the high stress concentration makes it difficult to obtain a refined picture of the stress field in the contact zone. First studies by the Finite Element method of the two-dimensional stresses beneath a cylindrical indenter were made by Akyuz & Merwin (1968). More complete computations for the indentation of an elastic-perfectly-plastic half-space by a cylinder and sphere have been presented by Hardy *et al.* (1971), Dumas & Baronet (1971), Lee *et al.* (1972) and Skalski (1979). They follow the development of the plastic zone as the load is increased and more elements of the mesh reach the elastic limit. Computational difficulties arose when the fully plastic state was approached and the calculations were restricted to a load $P < 100P_Y$, where P_Y is the load for first yield. These difficulties have been overcome by Follansbee & Sinclair (1984) for ball indentation of a strain-hardening solid well into the fully plastic state.

The pressure distributions found by Hardy *et al.* are shown in Fig. 6.11. As expected, plastic flow leads to a flattening of the pressure distribution and at high loads may peak slightly towards the edge. The development of the plastic zone is also shown. It roughly follows the contours of J_2 (defined by eq. (6.1)) and, for the range of loads investigated, is almost completely contained beneath the contact area.

An alternative approach to the analysis of an elastic-plastic indentation, which avoids the numerical complexities of finite elements, follows an early suggestion of Bishop, Hill & Mott (1945), which was developed by Marsh (1964) and Johnson (1970*a*). It is based on the observations of Samuels & Mulhearn (1956) and Mulhearn (1959) that the subsurface displacements produced by any blunt indenter (cone, sphere or pyramid) are approximately radial from the point of first contact, with roughly hemi-spherical contours of equal strain (Fig. 6.12).

In this simplified model of an elastic-plastic indentation we think of the contact surface of the indenter being encased in a hemi-spherical 'core' of radius a (Fig. 6.13). Within the core there is assumed to be a hydrostatic component of stress $\bar{p}$. Outside the core it is assumed that the stresses and displacements have radial symmetry and are the same as in an infinite elastic, perfectly-plastic body which contains a spherical cavity under a pressure $\bar{p}$. The elastic-plastic boundary lies at a radius c, where $c > a$. At the interface between core and the plastic zone (a) the hydrostatic stress in the core is just equal to the radial component of stress in the external zone, and (b) the radial

Fig. 6.11. Indentation of an elastic-plastic half-space by a rigid sphere, Hardy *et al.* (1971): development of the plastic zone. Broken line – contours of J_2.

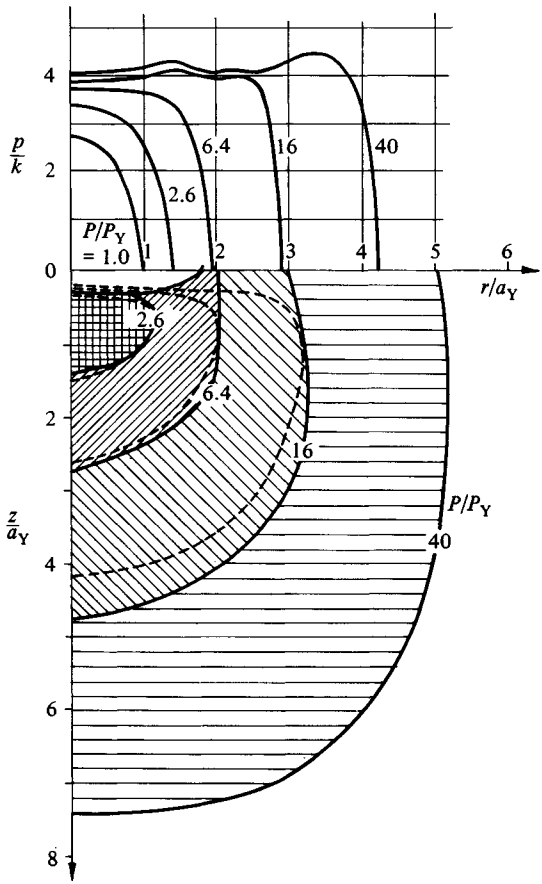

https://doi.org/10.1017/CBO9781139171731.007 Published online by Cambridge University Press

displacement of particles lying on the boundary $r = a$ during an increment of penetration dh must accommodate the volume of material displaced by the indenter (neglecting compressibility of the core).

The stresses in the plastic zone $a \leqslant r \leqslant c$ are given by (Hill, 1950*a*, p. 99):

$$\sigma_r/Y = -2\ln(c/r) - 2/3 \tag{6.30a}$$

$$\sigma_\theta/Y = -2\ln(c/r) + 1/3 \tag{6.30b}$$

In the elastic zone $r \geqslant c$

$$\sigma_r/Y = -\tfrac{2}{3}(c/r)^3, \quad \sigma_\theta/Y = \tfrac{1}{3}(c/r)^3 \tag{6.31}$$

Fig. 6.12. Experimental contours of plastic strain produced by (*a*) ball indentation ($a/R = 0.51$) and (*b*) Vicker's hardness pyramid indenter.

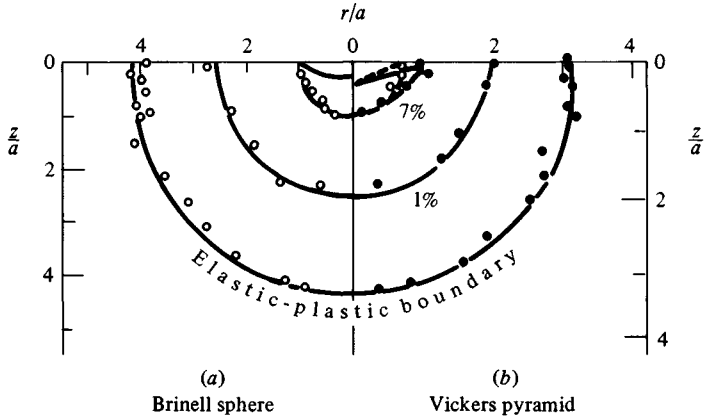

Fig. 6.13. Cavity model of an elastic-plastic indentation by a cone.

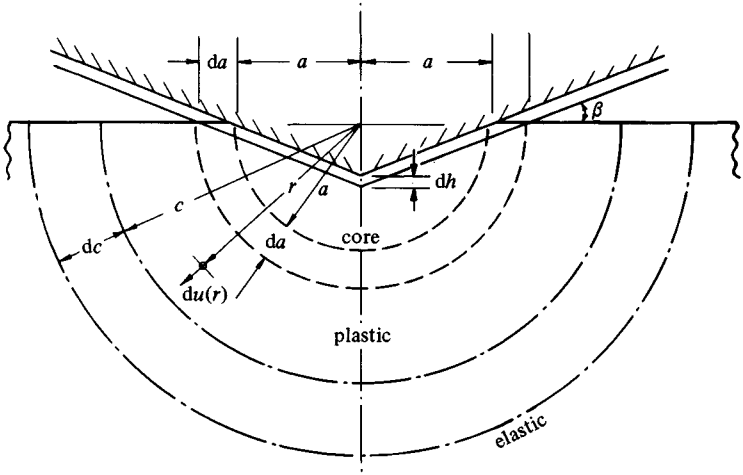

https://doi.org/10.1017/CBO9781139171731.007 Published online by Cambridge University Press

At the boundary of the core, the core pressure is given by

$$\bar{p}/Y = -[\sigma_r/Y]_{r=a} = 2/3 + 2\ln(c/a) \tag{6.32}$$

The radial displacements are given by (Hill, 1950, p. 101)

$$\frac{\mathrm{d}u(r)}{\mathrm{d}c} = \frac{Y}{E}\{3(1-\nu)(c^2/r^2) - 2(1-2\nu)(r/c)\} \tag{6.33}$$

Conservation of volume of the core requires

$$2\pi a^2\,\mathrm{d}u(a) = \pi a^2\,\mathrm{d}h = \pi a^2 \tan\beta\,\mathrm{d}a \tag{6.34}$$

where β is the inclination of the face of the cone to the surface ($\beta = \pi/2 - \alpha$). If we put $r = a$ in (6.33) and note that for a conical indenter geometrical similarity of the strain field with continued penetration requires that $\mathrm{d}c/\mathrm{d}a = c/a =$ constant, then equations (6.33) and (6.34) locate the elastic-plastic boundary by

$$E\tan\beta/Y = 6(1-\nu)(c/a)^3 - 4(1-2\nu) \tag{6.35}$$

Substitution for (c/a) in (6.32) gives the pressure in the core. For an incompressible material a simple expression is obtained:

$$\frac{\bar{p}}{Y} = \tfrac{2}{3}\left\{1 + \ln\left(\tfrac{1}{3}\frac{E\tan\beta}{Y}\right)\right\} \tag{6.36}$$

Of course the stress in the material immediately below an indenter is not purely hydrostatic. If $\bar{p}$ denotes the hydrostatic component, the normal stress will have a value $\sigma_z \approx -(\bar{p} + 2Y/3)$ and the radial stress $\sigma_r \approx -(\bar{p} - Y/3)$. A best estimate of the indentation pressure p_m for the spherical cavity model would therefore be $\bar{p} + 2Y/3$. A similar analysis may be made for two-dimensional indentation by a rigid wedge (Johnson, 1970*a*).

It appears from equation (6.36) that the pressure in the hydrostatic core beneath the indenter is a function of the single non-dimensional variable $E\tan\beta/Y$, which may be interpreted as the ratio of the strain imposed by the indenter ($\tan\beta$) to the elastic strain capacity of the material (Y/E). Elasticity of the indenter can be taken into account by replacing E by E^* (as defined in §4.2(*a*)).

The indentation pressure under elastic, elastic-plastic and fully plastic conditions may be correlated on a non-dimensional graph of p_m/Y as a function of $(E^*\tan\beta/Y)$ where β is the (small) angle of the indenter at the edge of the contact (Fig. 6.14). With a spherical indenter we put $\tan\beta \approx \sin\beta = a/R$ which varies during the indentation. Integration of equations (6.33) and (6.34), with $c/a = 1$ at the point of first yield ($p_m = 1.1Y$), leads to equation (6.36) with an additional constant (≈ 0.19) on the right-hand side. For a Vickers diamond pyramid, β is taken to be the angle of the cone (19.7°) which displaces the

https://doi.org/10.1017/CBO9781139171731.007 Published online by Cambridge University Press

same volume. First yield for a spherical indenter occurs at $p_m \approx 1.1Y$ and for a conical indenter at $p_m \approx 0.5Y$. Fully plastic deformation sets an upper limit of $\sim 3Y$ for the indentation pressure which is reached at a value of $(E^* \tan \beta/Y)$ ≈ 30 for a cone and $(E^*a/YR) \approx 40$ for a sphere.

The discussion above has been restricted to elastic-perfectly-plastic solids having a constant yield stress Y in simple compression. Tabor (1951) has shown that the results for a perfectly plastic solid may be applied with good approximation to a strain-hardening solid if Y is replaced by a 'representative' flow stress Y_R, measured in simple compression at a representative strain ϵ_R, where

$$\epsilon_R \approx 0.2 \tan \beta \tag{6.37}$$

For a Vickers hardness pyramid, therefore, $\epsilon_R \approx 0.07$ (Tabor suggested 0.08) and for a spherical indenter, $\epsilon_R \approx 0.2a/R$. Matthews (see §6) has considered materials which strain-harden according to a power law of index n, with the result $\epsilon_R = 0.28(1 + 1/n)^{-n}(a/R)$, which varies slightly with n from $0.17a/R$ to $0.19a/R$. In this way good agreement is found between elastic-perfectly-

Fig. 6.14. Indentation of an elastic-plastic half-space by spheres and cones. Small-dashed line – elastic: A cone, B sphere. Solid line – finite elements: C Hardy *et al.* (1971), D Follansbee & Sinclair (1984). Chain line – cavity model: F cone, G sphere. Large-dashed line – rigid-plastic (sphere), E Richmond *et al.* (1974). Experiments: cross – pyramids, Marsh (1964), circle – spheres, Tabor (1951).

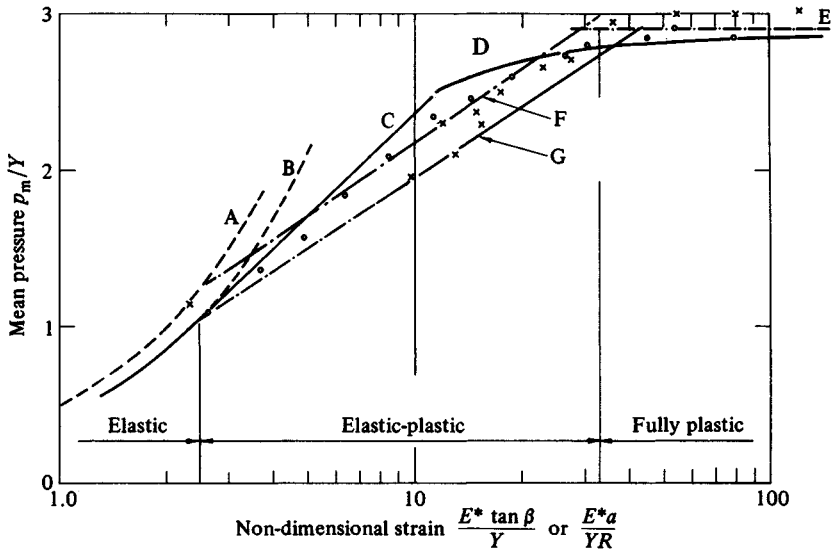

https://doi.org/10.1017/CBO9781139171731.007 Published online by Cambridge University Press

plastic theory and experiments on strain-hardening materials. Thus Fig. 6.14 gives a measure of the mean indentation pressure by an axi-symmetrical indenter of arbitrary profile pressed into any elastic-plastic solid whose stress-strain curve in simple compression is known. In particular it gives a relationship between hardness and the flow stress in simple compression. Thus the Vickers diamond pyramid hardness H_V is given by

$$H_V = 0.93p_m \approx 2.8Y_R \tag{6.38}$$

where Y_R is the flow stress in simple compression at a strain of about 0.08.

Experimental data for spherical indentation of various materials have been examined by Francis (1976) and been shown to correlate well using the variables defined above.

For a fully plastic spherical indentation ($(E^*a/YR) = 170$), the stresses along the z-axis and close to the surface found by the finite element method (Follansbee & Sinclair, 1984) (1) are compared in Figs. 6.15 and 6.16 with (2) rigid-plastic theory for a rigid punch and (3) the spherical cavity model. The general agreement between the rigid-plastic theory and the finite element analysis theory is good, particularly when it is remembered that the latter was carried out for a strain-hardening material. Adhesion at the face of the punch causes the maximum values of σ_r and σ_z to be located beneath the surface, an effect which is

Fig. 6.15. Plastic indentation by a rigid sphere, subsurface stresses, (A) frictionless, and (B) adhesive. (1) Finite elements, Follansbee & Sinclair (1984). (2) Rigid-plastic punch, Shield (1955), Eason & Shield (1960). (3) Cavity model, eqs. (6.30) and (6.31).

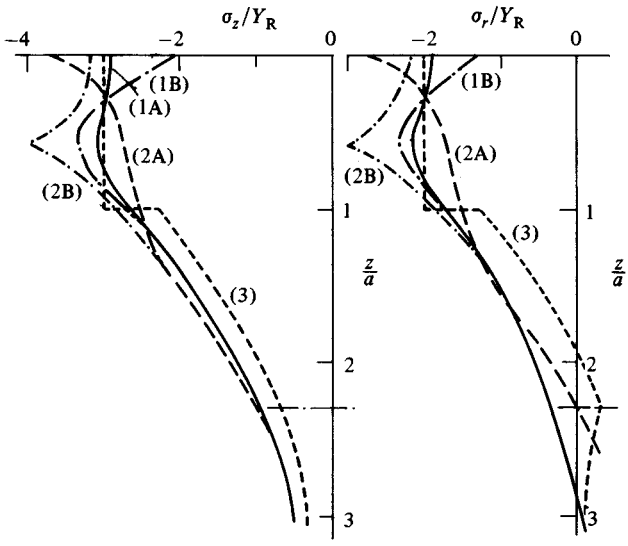

https://doi.org/10.1017/CBO9781139171731.007 Published online by Cambridge University Press

also apparent in the finite elements results. For the spherical cavity model, in the fully plastic state $p_m/Y = 3; E^* \tan\beta/Y = 40$ whereupon equation (6.35) gives the elastic-plastic boundary at $c/a \approx 2.3$. The stresses are then given by equations (6.30) and (6.31). Along the z-axis they show the same trend as the finite elements but underestimate their magnitude. On the surface, the cavity model predicts circumferential *tension* and radial *compression* for $r > 2a$. This is the opposite of the elastic state of stress in which the radial stress is tensile. The finite element calculations also show circumferential tension but of rather smaller magnitude. Rigid-plastic theory gives $\sigma_\theta = \sigma_z = 0$ (the Haar-von Kármán condition) as a result of using the Tresca yield criterion. The change from radial tension under purely elastic conditions to circumferential tension under elastic-plastic conditions is largely responsible for the change in the mode of indentation fracture from a ring crack with very brittle materials such as glass to a radial crack in semi-brittle materials such as perspex (Puttick *et al.*, 1977). Porous materials behave differently. They respond to indentation by crushing and the indentation pressure is of order Y, where Y is the crushing strength in uni-axial compression (see Wilsea *et al.*, 1975).

In addition to the contact pressure, the depth of penetration of the indenter is also of interest. It is a difficult quantity to determine theoretically, because of the uncertain 'pile-up' at the edge of the indentation. With a rigid-plastic solid the material displaced by the indenter appears in the piled-up shoulder, but with an elastic-plastic solid this is not the case. Most, if not all, of the displaced material is accommodated by radial expansion of the elastic hinterland.

Fig. 6.16. Plastic indentation by a rigid sphere, surface stresses. Legend as for Fig. 6.15.

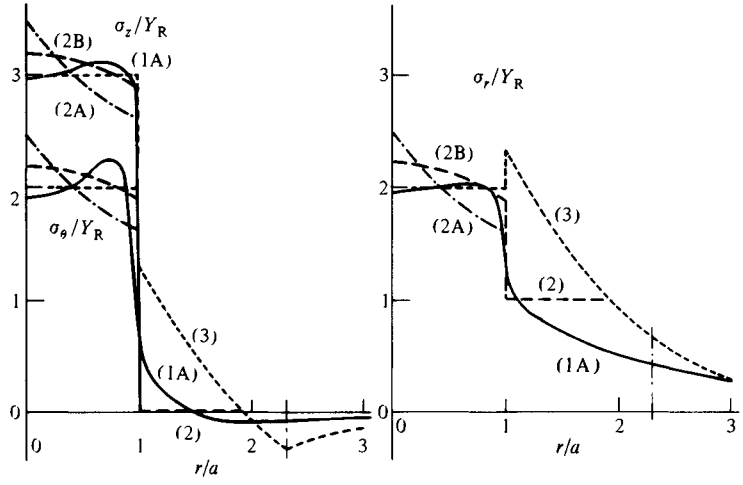

https://doi.org/10.1017/CBO9781139171731.007 Published online by Cambridge University Press

It reappears in an imperceptible increase in the external dimensions of the indented body. Pile-up is also influenced by the strain-hardening properties of the material. A large capacity for strain hardening pushes the plastic zone further into the material and thereby decreases the pile-up adjacent to the indenter.

A plot of penetration δ against load P is usually referred to as a compliance curve. Suitable non-dimensional variables for a spherical indenter are:

$$\delta/\delta_Y \equiv 0.148(\delta E^{*2}/RY^2) \tag{6.39a}$$

and

$$P/P_Y \equiv 0.043(PE^{*2}/R^2Y^3) \tag{6.39b}$$

where the load at first yield P_Y is given by equation (6.10) and the corresponding displacement δ_Y is related to P_Y by the elastic equation (4.23). The fully plastic condition is reached when $E^*a/RY \approx 40$, i.e. when $P/P_Y \approx 400$. If, in the fully plastic regime, it is assumed that the edges of the impression neither pile up nor sink in, then the penetration is given approximately by†

$$\delta = a^2/2R \tag{6.40}$$

Taking the fully plastic contact pressure to be $3.0Y$ and constant, this gives

$$P/P_Y = 0.81(\delta E^{*2}/RY^2) = 5.5(\delta/\delta_Y) \tag{6.41}$$

Accurate measurements of penetration are not so easy to obtain as those of contact pressure. Measurements by Foss & Brumfield (1922) of the penetration under load and the depth of the residual crater are plotted non-dimensionally‡ in Fig. 6.17. On the basis of the non-dimensional variables (6.39) the results for materials of different hardness and elastic modulus lie on a common curve which approaches the elastic line at light loads and equation (6.41) in the fully plastic regime.

6.4 Unloading of a plastic indentation, cyclic loading and residual stresses

The contact of *elastic* solids loaded by a normal force, discussed in detail in Chapters 4 and 5, is generally regarded as a reversible process. The stresses and deformation produced by a specific contact load are then independent of the history of loading. Small departures from perfect reversibility, however, can arise in two ways; by slip and friction at the contact interface, or by internal hysteresis of the materials under the action of cyclic stress.

If the materials of two contacting bodies are dissimilar, we have seen in §5.4 that some slip occurs at the periphery of the contact area. During unloading

† An expression for δ which takes account of strain hardening is given by equation (6.82).

‡ Since Foss & Brumfield quote hardness H rather than yield stress of their specimens, Y has been taken as $H/2.8$.

https://doi.org/10.1017/CBO9781139171731.007 Published online by Cambridge University Press

the direction of slip will reverse and the tangential surface traction will differ from that during loading. The contact force to produce a given contact area will be slightly greater during loading than during unloading. In a complete load cycle a small amount of energy is dissipated through interfacial slip. Although precise calculations have not been made it is clear that this energy dissipation is very small. The difference in the bulk stresses between loading and unloading will be negligible although in a situation of rapid cyclic loading the interfacial slip itself and the heat generated may be responsible for progressive surface damage.

Fig. 6.17. Penetration of a spherical indenter into an elastic-plastic half-space. Solid line – penetration under load. Broken line – depth of unloaded crater.

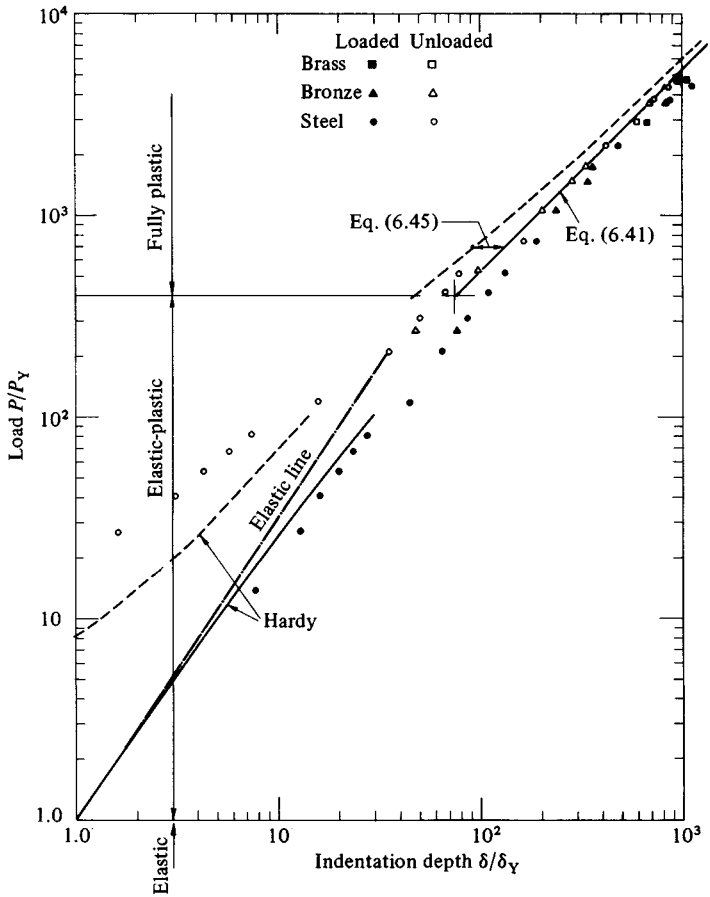

https://doi.org/10.1017/CBO9781139171731.007 Published online by Cambridge University Press

Real materials, even metals below their yield point, are not perfectly elastic, but exhibit some hysteresis during a cycle of stress. Such 'elastic hysteresis' or 'internal damping' gives rise to a slight irreversibility in a contact stress cycle. Provided that the departure from perfect elasticity is small the effect upon the overall distribution of contact stress will be small. An estimate of the energy dissipated in one cycle of the load may be made. The usual way of expressing the internal hysteresis of a material is by the ratio of the energy dissipated per cycle ΔW to the maximum elastic strain energy in the cycle W. This ratio $\alpha(= \Delta W/W)$ is known as the *hysteresis-loss factor* or the *specific damping capacity*. Representative values for a wide variety of materials are quoted by Lazan (1968). The damping capacity of most materials depends upon the amplitude of cyclic strain; the values tend to rise as the elastic limit is approached, but are roughly constant at low and moderate strains.

The elastic strain energy when two bodies are in contact can be calculated from the relationship between load and compression, thus

$$W = \int P \, \mathrm{d}\delta$$

For two spherical surfaces the relationship between P and δ is given by equation (4.23) for which

$$W = \tfrac{2}{5}\left(\frac{9E^{*2}P^5}{16R}\right)^{1/3} \tag{6.42}$$

The energy loss in a load cycle from zero to a maximum and back to zero is then given approximately by

$$\Delta W = \alpha W$$

where α is a representative value of the hysteresis-loss factor. Direct measurements by the author of the energy loss in the cyclic normal contact of spheres over a range of loads yielded a fairly constant value of α equal to 0.4% for a hard bearing steel. This value is not inconsistent with internal hysteresis measurements at high stress.

When the initial loading takes the material well into the plastic range the above approach is no longer appropriate, since the differences between loading and unloading will no longer be small. Even though large plastic deformations occur during loading, however, it is intuitive to expect the unloading process to be perfectly elastic. A simple check of this hypothesis was carried out by Tabor (1948) from observations of the permanent indentations made by a hard steel ball of radius R in the flat surface of a softer metal (see Fig. 6.18). The indentation under load has a radius R', which is slightly greater than R due to elastic compression of the ball (Fig. 6.18(*b*)). When the load is removed the plastic

https://doi.org/10.1017/CBO9781139171731.007 Published online by Cambridge University Press

indentation shallows to some extent due to elastic recovery, so that its permanent radius ρ is slightly greater than R' (Fig. 6.18(*c*)). If the unloading process is elastic, and hence reversible, a second loading of the plastic indentation will follow the elastic process in which a ball of radius R is pressed into contact with a concave spherical cup of radius ρ. Provided that the indentation is not too deep, so that the assumptions of the Hertz theory still apply, the permanent radius of the indentation can be related to the radius of the ball by equation (4.22). Remembering that ρ, being concave, is negative,

$$4a^3\left(\frac{1}{R}-\frac{1}{\rho}\right)=3P/E^* \tag{6.43}$$

Tabor's measurements of ρ were consistent with this equation to the accuracy of the observations.

The elastic deflexion which is recovered when the load is removed can be estimated in the same way. By eliminating R from the elastic equations (4.22) and (4.23), the elastic deflexion δ' can be expressed in terms of the mean contact pressure p_m by

$$\delta'^2=\frac{9\pi}{16}\frac{Pp_m}{E^{*2}} \tag{6.44}$$

In the fully plastic state $p_m \approx 3.0Y$, so that equation (6.44) can then be written, in terms of the non-dimensional variables of equation (6.41), as

$$P/P_Y = 8.1\times10^{-3}(\delta' E^{*2}/RY^2)^2 = 0.38(\delta'/\delta_Y)^2 \tag{6.45}$$

The residual depth of the indentation after the load is removed is therefore $(\delta-\delta')$. In the fully plastic range it may be estimated from equations (6.41) and (6.45) resulting in the line at the right-hand side of Fig. 6.17. The residual depth calculated by the finite element analysis is plotted at the left-hand side of Fig. 6.17. It appears that the elastic recovery given by equation (6.45) is in good agreement with Foss & Brumfield's measurements.

Fig. 6.18. Unloading a spherical indenter. (*a*) before loading, (*b*) under load, (*c*) after unloading.

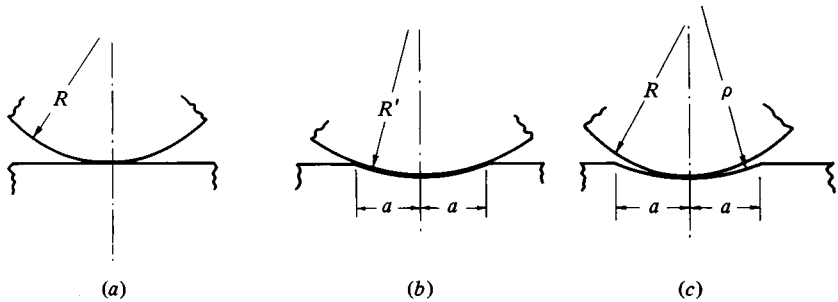

https://doi.org/10.1017/CBO9781139171731.007 Published online by Cambridge University Press

A similar investigation of the unloading of conical indenters (Stilwell & Tabor, 1961)) showed that the shallowing of the indentation could be ascribed to elastic recovery and calculated from the elastic theory of cone indentation (§5.2).

This treatment of the unloading process is only approximate, however, since it tacitly assumes that the pressure distribution before unloading is Hertzian and hence that the recovered profile is a circular arc. The actual pressure distribution is flatter than that of Hertz as shown in Fig. 6.11. This pressure distribution, when released by unloading, will give rise to an impression whose profile is not exactly circular, but whose shape is related to the pressure by the elastic displacement equations. Hence, accurate measurement of the recovered profile enables the actual pressure distribution before unloading to be deduced. This has been done by Johnson (1968*b*) for copper spheres and cylinders and by Hirst & Howse (1969) for perspex indented by a hard metal wedge.

After unloading from a plastically deformed state the solid is left in a state of residual stress. To find the residual stress it is first necessary to know the stresses at the end of the plastic loading. Then, assuming unloading to be elastic, the residual stresses can be found by superposing the elastic stress system due to a distribution of surface normal traction equal and opposite to the distribution of contact pressure. The contact surface is left free of traction and the internal residual system is self-equilibrating. Such calculations have been made in detail by the finite element method (Hardy *et al.*, 1971; Follansbee & Sinclair, 1984). They show that the material beneath the indenter is left in a state of residual compression and the surface outside the impression contains radial compression and circumferential tension.

The residual stresses left in the solid after a fully plastic indentation may be estimated using the slip-line field solutions or the spherical cavity model. A rough idea what to expect can be gained by simple reasoning: during a plastic indentation the material beneath the indenter experiences permanent compression in the direction perpendicular to the surface and radial expansion parallel to the surface. During the recovery, the stress normal to the surface is relieved, but the permanent radial expansion of the plastically deformed material induces a radial compressive stress exerted by the surrounding elastic material. The shot-peening process, which peppers a metal surface with a large number of plastic indentations, gives rise to a residual bi-axial compressive stress, acting parallel to the surface, whose intensity is greatest in the layers just beneath the surface. The aim of the process is to use the residual compression in the surface layers to inhibit the propagation of fatigue cracks.

Along the axis of symmetry, during plastic loading

$$|\sigma_z - \sigma_r| = Y \tag{6.46}$$

https://doi.org/10.1017/CBO9781139171731.007 Published online by Cambridge University Press

During *elastic* unloading,

$$|\sigma_r - \sigma_z| = Kp_m = KcY \tag{6.47}$$

where K depends upon the pressure distribution at the end of loading and upon the depth below the surface. The residual stress difference is then given by the superposition of (6.46) and (6.47), i.e.

$$|\sigma_r - \sigma_z|_r = (Kc - 1)Y \tag{6.48}$$

Since $(\sigma_z)_r$ is zero at the surface, its value beneath the surface is likely to be small compared with $(\sigma_r)_r$. In a fully plastic indentation $c \approx 3.0$ and the pressure distribution is approximately uniform which, by equation (3.33), gives $K = 0.65$ at $z = 0.64a$. Hence $(Kc - 1) \approx 0.95$ so that, from equation (6.48), reversed yielding on unloading is not to be expected except as a consequence of the Bauchinger effect. Even if some reversed yielding does take place it will be fully contained and its influence on the surface profile will be imperceptible.

At the contact surface the situation is different, taking the pressure p to be uniform, $\sigma_z = -p$, $\sigma_r = \sigma_\theta = -(p - Y)$. Elastic unloading superposes stresses $\sigma_z = p$, $\sigma_r = \sigma_\theta = \frac{1}{2}(1 + 2\nu)p \approx 0.8p$, leaving residual stresses

$$(\sigma_z)_r = 0, \quad (\sigma_r)_r = (\sigma_\theta)_r = Y - 0.2p \tag{6.49}$$

Putting $p = 3Y$ for a fully plastic indentation gives $(\sigma_r)_r = (\sigma_\theta)_r \approx 0.4Y$ which is *tensile.*

At the surface in the plastic zone outside the contact area the stresses due to loading are given approximately by the cavity model (eqs. (6.30) and (6.31)). The radial stress is compressive and the circumferential stress though small is tensile. Elastic unloading would add

$$\sigma_r = -\sigma_\theta = -\tfrac{1}{2}(1 - 2\nu)p_m a^2/r^2$$

but additional radial compression and circumferential tension are not possible. Instead slight additional plastic deformation will occur whilst the stresses remain roughly constant. Subsequent loading and unloading will then be entirely elastic.

6.5 Linear viscoelastic materials

Many materials, notably polymers, exhibit time-dependent behaviour in their relationships between stress and strain which is described as viscoelastic. The common features of viscoelastic behaviour are illustrated in Fig. 6.19 which shows the variation of strain $\epsilon(t)$ in a specimen of material under the action of a constant stress σ_0 applied for a period t_1. The strain shows an *initial elastic response OA* to the applied stress; a further *delayed elastic strain AB* is acquired in time. If the material is capable of flow or creep it will also acquire a steadily increasing *creep strain BC.* When the stress is removed there is an immediate elastic response *CD* ($= -OA$) and a delayed elastic response *DE.* The specimen is left with a permanent strain at E which it acquired through the action of creep.

https://doi.org/10.1017/CBO9781139171731.007 Published online by Cambridge University Press

This material behaviour can be incorporated into a rigorous theory of contact stresses provided that the viscoelastic stress-strain relationships of the material can be taken to be *linear.* For this requirement to be met, the strains must remain small (as in the linear theory of elasticity) and the principle of superposition must apply. Thus, for linearity, an increase in the stress in Fig. 6.19 by a constant factor must produce an increase in the strain response by the same factor; further, the strain response to different stress histories, acting simultaneously, must be identical to the sum of the responses to the stress histories applied separately. The stress-strain relations for a linear viscoelastic material can be expressed in various ways, but the most common is to make use of the *creep compliance function* which expresses the strain response to a step change in stress or, alternatively, the *relaxation function* which expresses the stress response to a step change in strain. An isotropic material in a state of complex stress requires two independent functions to express its response to shear and volumetric deformation respectively. These functions correspond to the shear modulus and bulk modulus of purely elastic solids. For simplicity, in what follows, we shall restrict our discussion to an incompressible material so that its stress-strain relations can be expressed in terms of a single function describing its behaviour in shear.† The approximation is a reasonable one for polymers, whose values of Poisson's ratio usually exceed 0.4. It is convenient to write the stress-strain relations in terms of the deviatoric stress components $s = (\sigma - \bar{\sigma})$ and the deviatoric strains $e = (\epsilon - \bar{\epsilon})$ where $\bar{\sigma} = \frac{1}{3}(\sigma_1 + \sigma_2 + \sigma_3)$ and

† An alternative simplification is to assume that Poisson's ratio remains constant with time in which case the relaxation functions in response to volumetric and shear deformations are in the fixed ratio of $2(1 + \nu)/3(1 - 2\nu)$.

Fig. 6.19

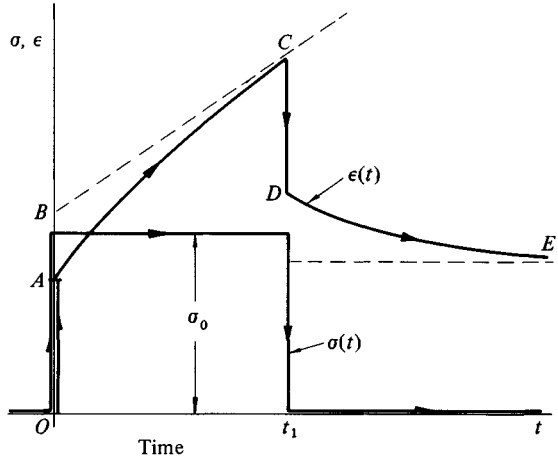

https://doi.org/10.1017/CBO9781139171731.007 Published online by Cambridge University Press

$\bar{\epsilon} = \frac{1}{3}(\epsilon_1 + \epsilon_2 + \epsilon_3)$. For an incompressible elastic solid $\bar{\epsilon} = 0$, so that

$$s = 2Ge = 2G\epsilon \tag{6.50}$$

where G is the shear modulus. The corresponding relationship for an incompressible viscoelastic material may be written as either

$$s(t) = \int_0^t \Psi(t - t') \frac{\partial e(t')}{\partial t'} \, dt' \tag{6.51}$$

or

$$e(t) = \int_0^t \Phi(t - t') \frac{\partial s(t')}{\partial t'} \, dt' \tag{6.52}$$

The function $\Psi(t)$ is the relaxation function, which specifies the stress response to a unit step change of strain; the function $\Phi(t)$ is the creep compliance, which specifies the strain response to a unit step change in stress. For particular materials, they may be deduced from appropriate spring and dashpot models or obtained by experiment (see Lee & Rogers, 1963). Equation (6.51), expressed in terms of the relaxation function $\Psi(t)$, can be regarded as the superposition of the stress responses to a sequence of small changes of strain $de(t')$ at times t'. Similarly equation (6.52) expresses the total strain response to a sequence of step changes in stress.

By way of example we shall make use of two idealised viscoelastic materials which demonstrate separately the effects of delayed elasticity and steady creep. The first material is represented in Fig. 6.20(*a*) by two springs of modulus g_1 and g_2 together with a dashpot of viscosity η connected as shown. For this material the creep response to a step change is stress s_0 is given by

$$e(t) = \Phi(t)s_0 = \left[\frac{1}{g_1} + \frac{1}{g_2}\{1 - \exp(-t/T_1)\}\right] s_0 \tag{6.53}$$

where $T_1 = \eta/g_2$. The response to a step change of strain e_0 is given by

$$s(t) = \Psi(t)e_0 = \frac{g_1}{g_1 + g_2}\{g_2 + g_1 \exp(-t/T_2)\} \, e_0 \tag{6.54}$$

where $T_2 = \eta/(g_1 + g_2)$.

The second material - a Maxwell body - is represented in Fig. 6.20(*b*) by a spring of modulus g in series with a dashpot of viscosity η. The creep response is

$$e(t) = \Phi(t)s_0 = \left\{\frac{1}{g} + \frac{1}{\eta}t\right\} s_0 \tag{6.55}$$

and the relaxation response is

https://doi.org/10.1017/CBO9781139171731.007 Published online by Cambridge University Press

$$s(t) = \Psi(t)e_0 = ge^{-t/T}e_0 \tag{6.56}$$

where $T = \eta/g$ is the relaxation time of the material.

The first material exhibits delayed elasticity but the ultimate strain is limited to a finite value. The second material shows a steady creep under constant stress, so that the strains increase continuously with time. Of course this model is only valid during time intervals when the strains remain small. For the Maxwell model to be representative of a 'solid' rather than a 'fluid', the viscosity η must be large, comparable in magnitude with the modulus of elasticity g. The simplest model of a material which exhibits both delayed elasticity and steady creep is made up of four elements, by adding a second dashpot in series with the model shown in Fig. 6.20(*a*).

We shall now examine the behaviour when a rigid spherical indenter is pressed into contact with a viscoelastic solid. Under the action of a constant normal force the penetration of the indenter and the contact area will both grow with time and the distribution of contact pressure will change. In principle we wish to find, for a given material, the variation with time of the contact area and pressure distribution resulting from any prescribed programme of loading or penetration. The simplest approach to this problem follows a suggestion by Radok (1957) for

Fig. 6.20. Simple viscoelastic materials which display (*a*) delayed elasticity, (*b*) steady creep (Maxwell).

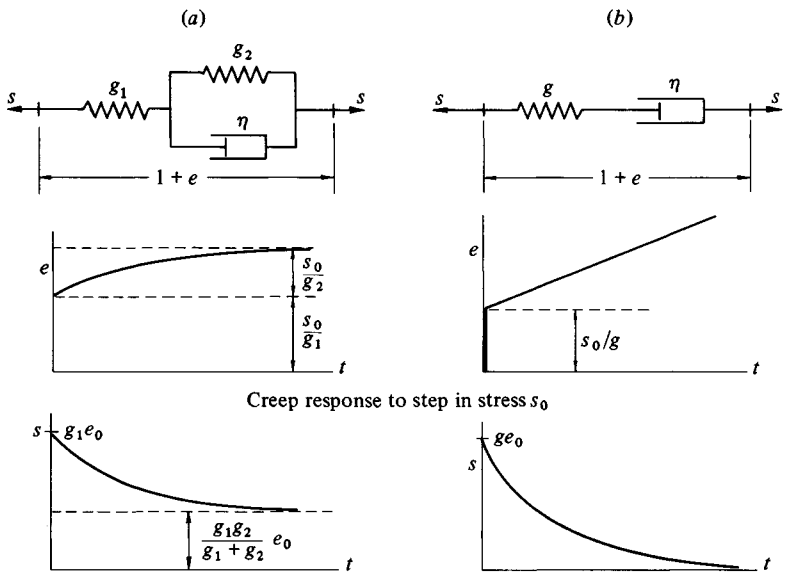

https://doi.org/10.1017/CBO9781139171731.007 Published online by Cambridge University Press

finding the stresses and deformations in cases where the corresponding solution for a purely elastic material is known.

It consists of replacing the elastic constant in the elastic solution by the corresponding integral operator from the viscoelastic stress–strain relations. If the deformation history is known, the stresses are found by replacing $2G$ in the elastic solution by the integral operator, expressed in terms of the relaxation function $\Psi(t)$ (eq. (6.51)). On the other hand, if the load or stress history is known, the variation in deformation is found from the elastic solution by replacing the constant $(1/2G)$ by the integral operator involving the creep compliance $\Phi(t)$ (eq. (6.52)). Lee & Radok (1960) show that this approach can be applied to the contact problem provided that the loading programme is such that the contact area is increasing throughout.

When two purely elastic spherical bodies are pressed into contact by a force P, the radius of the contact circle a, the penetration δ and the contact pressure p are given by equations (4.22), (4.23) and (4.24). If one sphere is rigid and the other is incompressible with a shear modulus G, these expressions for a and δ may be written:

$$a^3 = (R\delta)^{3/2} = \tfrac{3}{8}\left(\frac{1}{2G}\right)RP \tag{6.57}$$

and for the pressure distribution:

$$p(r) = \frac{4}{\pi R}\, 2G(a^2 - r^2)^{1/2} \tag{6.58}$$

where $1/R$ is the relative curvature of the two surfaces $(1/R_1 + 1/R_2)$. When the material is viscoelastic a and p vary with time so, following Radok's suggestion, we rewrite equation (6.58) for the pressure, replacing $2G$ by the relaxation operator for the material, thus for $r < a(t')$

$$p(r,t) = \frac{4}{\pi R}\int_0^t \Psi(t-t')\,\frac{\mathrm{d}}{\mathrm{d}t'}\{a^2(t') - r^2\}^{1/2}\,\mathrm{d}t' \tag{6.59}$$

Similarly the contact force is given by

$$P(t) = \frac{8}{3R}\int_0^t \Psi(t-t')\,\frac{\mathrm{d}}{\mathrm{d}t'}a^3(t')\,\mathrm{d}t' \tag{6.60}$$

If the variation of penetration $\delta(t)$ is prescribed, then the variation in contact radius $a(t)$ is given directly by the first of (6.57), i.e.

$$a^2(t) = R\delta(t)$$

which can be substituted in (6.59) to find the variation in pressure distribution. It is more common however, for the load variation $P(t)$ to be prescribed. In this

https://doi.org/10.1017/CBO9781139171731.007 Published online by Cambridge University Press

case we replace $(1/2G)$ in (6.57) by the creep compliance operator to obtain

$$a^3(t) = \tfrac{3}{8}R \int_0^t \Phi(t-t') \frac{\mathrm{d}}{\mathrm{d}t'} P(t')\, \mathrm{d}t' \tag{6.61}$$

The integral form of equations (6.59) and (6.61) may be interpreted as the linear superposition of small changes in $p(r)$ brought about by a sequence of infinitesimal step changes in δ or P. Lee & Radok (1960) show that the pressure distribution given in equation (6.59) produces normal displacements of the surface of the solid $\bar{u}_z(r, t)$ which conform to the profile of the rigid sphere within the contact area $(r \leqslant a)$ at all times, i.e.

$$\bar{u}_z(r, t) = \delta(t) - r^2/2R$$

for all t.

Some of the significant features of viscoelastic contact will now be illustrated by applying the above method of analysis to two particular cases: the response of each of the two idealised viscoelastic materials shown in Fig. 6.20 to a step load applied to a rigid sphere. Thus the variation in load is prescribed:

$$P(t) = 0, \quad t < 0; \quad P(t) = P_0, \quad t > 0.$$

For a single step, equation (6.61) becomes

$$a^3(t) = \tfrac{3}{8}RP_0\Phi(t), \quad t > 0 \tag{6.62}$$

(a) Material with delayed elasticity

The material characterised in Fig. 6.20(*a*) has the creep compliance $\Phi(t)$ given by equation (6.53), which can be substituted in equation (6.62) to give the variation in contact radius

$$a^3(t) = \tfrac{3}{8}RP_0 \left\{ \frac{1}{g_1} + \frac{1}{g_2}(1 - \mathrm{e}^{-t/T}) \right\} \tag{6.63}$$

Immediately the load is applied there is an instantaneous elastic response to give a contact radius $a_0 = (3RP_0/8g_1)^{1/3}$. The contact size then grows with time as shown by curve A in Fig. 6.21, and eventually approaches

$$a_1 = \{3RP_0(1/g_1 + 1/g_2)/8\}^{1/3}.$$

Initially the contact pressure follows the elastic distribution of the Hertz theory given by (6.58) with $2G = g_1$ and $a = a_0$. Finally the pressure distribution again approaches the elastic form with $2G = g_1g_2/(g_1 + g_2)$ and $a = a_1$. At intermediate times the pressure distribution can be found by substituting the relaxation function $\Psi(t)$ from (6.54) and $a(t)$ from (6.63) into equation (6.59) and performing the integrations. These computations have been carried out by Yang (1966) for $g_2 = g_1$; the results are plotted in Fig. 6.22. It is apparent that the pressure distribution is not very different from the Hertz distribution at any

https://doi.org/10.1017/CBO9781139171731.007 Published online by Cambridge University Press

Fig. 6.21. Growth of contact radius $a(t)$ due to a step load P_0 applied to a rigid sphere of radius R. (A) Three parameter solid (Fig. 6.20(a)) with $g_1 = g_2 = g$ and $T = \eta/2g$, (B) Maxwell solid with $T = \eta/g$, and (C) viscous solid, $T = 2\eta/g$.

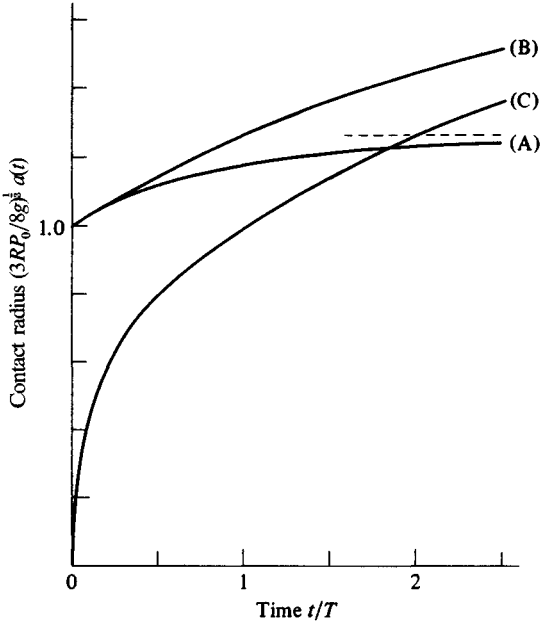

Fig. 6.22. Variation of pressure distribution when a step load is applied to a sphere indenting the 3-parameter solid of Fig. 6.20(A).

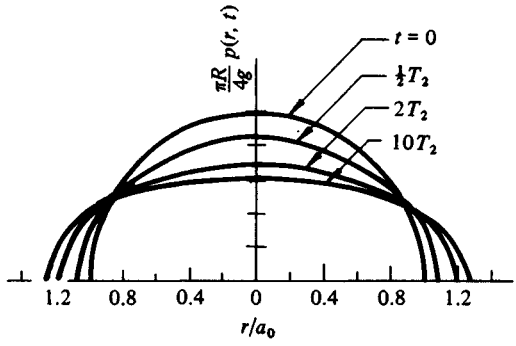

https://doi.org/10.1017/CBO9781139171731.007 Published online by Cambridge University Press

stage in the deformation. The effect of delayed elasticity, therefore, would seem to comprise a growth in the contact from its initial to its final size; the stresses at any instant in this process being distributed approximately according to elastic theory.

(b) Material with steady creep

The simplest material which exhibits steady creep is the Maxwell solid depicted in Fig. 6.20(*b*). The growth of contact size produced by a step load is found by substituting the creep compliance in (6.55) into equation (6.62) with the result

$$a^3(t) = \tfrac{3}{8}RP_0\left(\frac{1}{g}+\frac{1}{\eta}t\right) \tag{6.64}$$

Once again, the initial elastic deformation will give $a_0 = (3RP_0/8g)^{1/3}$ immediately the load is applied. The value of a will then grow continuously according to equation (6.64), as shown in Fig. 6.21, although it must be remembered that the theory breaks down when a becomes no longer small compared with R. Substituting the relaxation function $\Psi(t) = g\,e^{-t/T}$ from (6.56) together with (6.64) into equation (6.59) enables the variation in pressure distribution to be found. Numerical evaluation of the integral results in the pressure distributions shown in Fig. 6.23. The initial elastic response gives a Hertzian distribution of stress. As the material creeps the pressure distribution changes markedly. The growth of the contact area brings new material into the deformed region which responds elastically, so that, at the periphery of the contact circle, the pressure distribution continues to follow the Hertzian 'elastic' curve. In the centre of the contact the deformation does not change greatly, so that the stress relaxes which results in a region of low contact pressure. Thus, as time progresses, we see that the effect of continuous creep is to change the pressure distribution from the elastic form, in which the maximum pressure is in the centre of the contact area, to one where the pressure is concentrated towards the edge.

(c) Purely viscous material

It is interesting to observe that the phenomenon of concentration of pressure at the edge of contact arises in an extreme form when the material has no initial elastic response. A purely viscous material such as pitch, for example, may be thought of as a Maxwell material (Fig. 6.20(*b*)) in which the elastic modulus g becomes infinitely high. For such a material the stress response to a step change of strain - the relaxation function - involves a theoretically infinite stress exerted for an infinitesimally short interval of time. This difficulty can be avoided by rewriting the viscoelastic stress-strain relations (eq. (6.51)

and (6.52)) in terms of differential rather than integral operators. Thus a purely viscous material, with viscosity η (as usually defined), has the stress-strain relationship

$$s(t) = 2\eta \mathbf{D}e(t), \quad \text{where } \mathbf{D} \equiv \mathrm{d}/\mathrm{d}t. \tag{6.65}$$

Following Radok's method we can now replace G in the elastic solution by the differential operator $\mathbf{D}$. From the elastic equation (6.57) we get

$$a^3 = (R\delta)^{3/2} = \frac{3}{16\eta}\frac{1}{\mathbf{D}}RP$$

For the case of a step load, in which P has a constant value P_0 ($t > 0$),

$$a^3 = (R\delta)^{3/2} = \frac{3}{16}\frac{R}{\eta}P_0 t \tag{6.66}$$

The pressure distribution is obtained by replacing $2G$ by $2\eta\mathbf{D}$ in the elastic equation (6.58)

$$p(r,t) = \frac{8\eta}{\pi R}\mathbf{D}(a^2 - r^2)^{1/2}$$

$$= \frac{P_0}{2\pi a}(a^2 - r^2)^{-1/2} \tag{6.67}$$

Fig. 6.23. Variation of pressure distribution when a step load is applied to a sphere. Solid line – Maxwell fluid, $T = \eta/g$. Chain line – purely viscous fluid, $a^3 = 3a_0^3$. Broken line – elastic solid (Hertz).

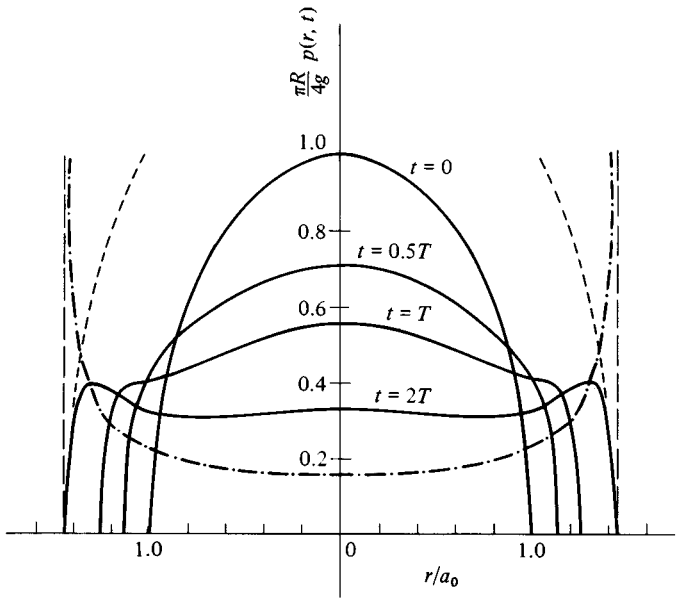

https://doi.org/10.1017/CBO9781139171731.007 Published online by Cambridge University Press

This pressure distribution maintains the same shape as the contact size grows; it rises to a theoretically infinite value at the periphery of the contact circle, as shown in Fig. 6.23. This result is not so surprising if it is remembered that, when the moving boundary of the contact circle passes an element of material in the surface, the element experiences a sudden jump in shear strain, which gives rise to the theoretically infinite stress. Other idealised materials which have no initial elastic response, for example a Kelvin solid (represented by the model in Fig. 6.20(*a*) in which the spring g_1 is infinitely stiff) would also give rise to an infinite pressure at the edge of the contact. Real solid-like materials, of course, will have sufficient elasticity to impose some limit to the edge pressures.

So far we have considered a rigid sphere indenting a viscoelastic solid: Yang (1966) has investigated the contact of two viscoelastic bodies of arbitrary profile. He shows that the contact region is elliptical and that the eccentricity of the ellipse is determined solely by the profiles of the two surfaces, as in the contact of elastic bodies, i.e. by equation (4.28). Further, the approach of the two bodies at any instant $\delta(t)$ is related to the size of the contact region, $a(t)$ and $b(t)$, at that instant by the elastic equations. When the material of both bodies is viscoelastic, the deformation of each surface varies with time in such a way that each body exerts an identical contact pressure on the other. In these circumstances equations (6.59) and (6.61) still yield the variations of contact pressure and contact size with time, provided that the relaxation and creep compliance functions $\Psi(t)$ and $\Phi(t)$ are taken to refer to a fictitious material whose elements may be thought of as a *series* combination of elements of the two separate materials. This procedure is equivalent to the use of the combined modulus E^* for elastic materials.

The method of analysis used in this section is based upon Radok's technique of replacing the elastic constants in the elastic solution by the corresponding integral or differential operators which appear in the stress-strain relations for linear viscoelastic materials. Unfortunately this simple technique breaks down when the loading history is such as to cause the contact area to *decrease* in size. Lee & Radok (1960) explain the reason for this breakdown. They show that, when their method is applied to the case of a shrinking contact area, negative contact pressures are predicted in the contact area. In reality, of course, the contact area will shrink at a rate which is different from their prediction such that the pressure will remain positive everywhere.

This complication has been studied by Ting (1966, 1968) and Graham (1967), with rather surprising conclusions. If, at time t, the contact size $a(t)$ is decreasing, a time t_1 is identified as that instant previously when the contact size $a(t_1)$ was increasing and equal to $a(t)$. It then transpires that the contact pressure $p(r, t)$

https://doi.org/10.1017/CBO9781139171731.007 Published online by Cambridge University Press

depends only upon the variation of contact size prior to t_1 during which it is less than $a(t)$. Hence equation (6.59) can still be used to find the contact pressure at time t, by making the limits of integration 0 and t_1. Equation (6.61) can be used to obtain $a(t')$, since the contact is increasing in the range $0 \leqslant t' \leqslant t_1$. The penetration $\delta(t)$, on the other hand, exhibits the opposite characteristics. During the period $0 \leqslant t' \leqslant t_1$, whilst $a(t')$ is increasing to $a(t_1)$, the penetration $\delta(t')$ is related to $a(t')$ by the elastic equation (6.57) and is not dependent upon the rate of loading. But when $a(t)$ is decreasing, the penetration $\delta(t)$ depends upon the time history of the variation of contact size during the interval from t_1 to t. For the relationship governing the variation of penetration with time when the contact area is shrinking, the reader is referred to the paper by Ting (1966).

If the loading history $P(t)$ is prescribed, the variation in contact size $a(t)$ may be found without much difficulty. As an example, we shall investigate the case of a rigid sphere pressed against a Maxwell material (Fig. 6.20(*b*)) by a force which increases from zero to a maximum P_0 and decreases again to zero, according to

$$P(t) = P_0 \sin (t/T) \tag{6.68}$$

as shown in Fig. 6.24. The material has an elastic modulus g and time constant $\eta/g = T$. Whilst the contact area is increasing its size is given by substituting the creep compliance of the material from (6.55) and the load history of (6.68) into equation (6.61), to give

$$\begin{aligned} a^3(t) &= \tfrac{3}{8}R \int_0^t \frac{1}{g} \{1 + (t - t')/T\} \frac{\partial P_0 \sin (t'/T)}{\partial t'} \, \mathrm{d}t' \\ &= \frac{3RP_0}{8g} \{\sin (t/T) - \cos (t/T) + 1\} \end{aligned} \tag{6.69}$$

This relationship only holds up to the maximum value of $a(t)$, which occurs at $t = t_m = 3\pi T/4$. When $a(t)$ begins to decrease we make use of the result that the contact pressure $p(r, t)$ and hence the total load $P(t)$ depend upon the contact stress history up to time t_1 only, where $t_1 \leqslant t_m$, and t_1 is given by

$$a(t_1) = a(t). \tag{6.70}$$

To find t_1, we use equation (6.60) for the load; and since the range of this integral lies within the period during which the contact size is increasing, we may substitute for $a^3(t')$ from equation (6.69) with the result that

$$\begin{aligned} P(t) &= P_0 \mathrm{e}^{-t/T} \int_0^{t_1/T} \mathrm{e}^{t'/T} \{\cos (t'/T) + \sin (t'/T)\} \, \mathrm{d}(t'/T) \\ &= P_0 \mathrm{e}^{-t/T} \mathrm{e}^{t_1/T} \sin (t_1/T) \end{aligned} \tag{6.71}$$

https://doi.org/10.1017/CBO9781139171731.007 Published online by Cambridge University Press

Since the load variation is known from (6.68), equation (6.71) reduces to

$$e^{t/T} \sin (t/T) = e^{t_1/T} \sin (t_1/T) \tag{6.72}$$

This equation determines t_1 corresponding to any given t. It is then used in conjunction with the relationship (6.69) to find $a(t)$ during the period when the contact is decreasing ($t > t_m$). The process is illustrated in Fig. 6.24 by plotting the function $e^{t/T} \sin (t/T)$.

From the figure we see that the maximum contact area is not coincident with the maximum load; the contact continues to grow by creep even when the load has begun to decrease. Only at a late stage in the loading cycle does the contact rapidly shrink to zero as the load is finally removed. The penetration of the sphere $\delta(t)$ also reaches a maximum at t_m. During the period of increasing indentation ($0 \leqslant t \leqslant t_m$), the penetration is related to the contact size by the elastic equation (6.57). During the period when the contact size is decreasing the penetration is greater than the 'elastic' value by an amount which depends upon

Fig. 6.24. Contact of a sphere with a Maxwell solid under the action of a sinusoidally varying force $P = P_0 \sin (t/T)$.

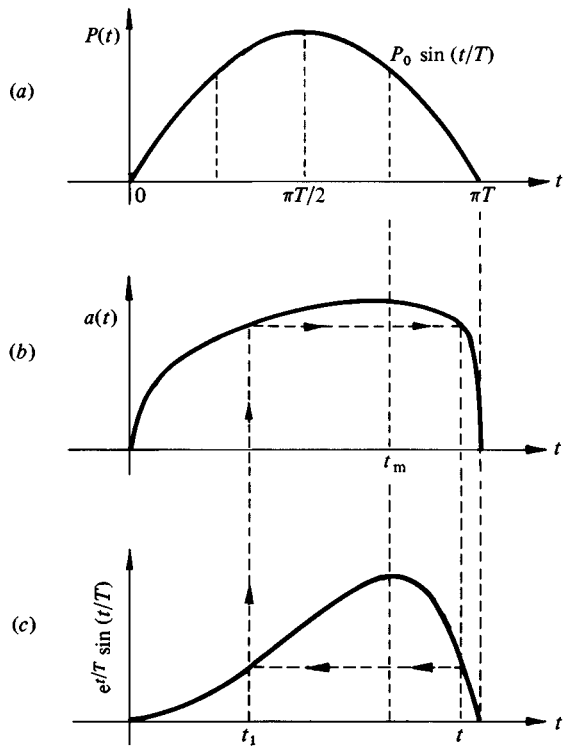

https://doi.org/10.1017/CBO9781139171731.007 Published online by Cambridge University Press

the detailed variation of $a(t)$ in this period. Thus an indentation remains at the time when the load and contact area have vanished.

The example we have just discussed is related to the problem of *impact* of a viscoelastic body by a rigid sphere. During impact, however, the force variation will be only approximately sinusoidal; it will in fact be related to the penetration, through the momentum equation for the impinging sphere. Nevertheless it is clear from our example that the maximum penetration will lag behind the maximum force, so that energy will be absorbed by the viscoelastic body and the coefficient of restitution will be less than unity. This problem has been studied theoretically by Hunter (1960) and will be discussed further in §11.5(*c*).

6.6 Nonlinear elasticity and creep

Many materials, particularly at elevated temperatures, exhibit nonlinear relationships between stress, strain and strain rate. Rigorous theories of nonlinear viscoelasticity do not extend to the complex stress fields at a nonconforming contact, but some simplified analytical models have proved useful. Two related cases have received attention: (i) a nonlinear elastic material with the power law stress–strain relationship

$$\epsilon = \epsilon_0(\sigma/\sigma_0)^n \tag{6.73}$$

and (ii) a material which creeps according to the power law:

$$\dot{\epsilon} = \dot{\epsilon}_0(\sigma/\sigma_0)^n = B\sigma^n \tag{6.74}$$

where σ_0, ϵ_0 and $\dot{\epsilon}_0$ are representative values of stress, strain and strain rate which, together with the index n, may be found by fitting the above relationships to uniaxial test data. The most frequent use of this nonlinear elastic model is to describe the *plastic* deformation of an annealed metal which severely strain-hardens. The model only applies, of course, while the material is being loaded, i.e. when the principal strain increments satisfy the condition

$$\{(d\epsilon_1 - d\epsilon_2)^2 + (d\epsilon_2 - d\epsilon_3)^2 + (d\epsilon_3 - d\epsilon_1)^2\} > 0$$

By taking values of n from 1 to ∞ a range of material behaviour can be modelled from linear elastic, in which Young's modulus $E = \sigma_0/\epsilon_0$, to rigid-perfectly-plastic in which yield stress $Y = \sigma_0$ (Fig. 6.25). The power law creep relationship (6.74) applies to the steady-state or 'secondary' creep of metals at elevated temperatures, provided the strain rate is less than about 10^{-2} s^{-1}.

Concentrated line load

The stresses and deformation produced by a concentrated normal line load acting on a half-space which deforms according to either of the constitutive laws (6.73) or (6.74) can be found exactly. This is the nonlinear analogue of the

https://doi.org/10.1017/CBO9781139171731.007 Published online by Cambridge University Press

linear elastic problem considered in §2.2. For a nonlinear elastic material the stress system was shown by Sokolovskii (1969) to be (in the notation of Fig. 2.2)

$$\sigma_r = -\frac{P}{D}(\cosh k\theta)^{1/n} \tag{6.75}$$

$$\sigma_\theta = \tau_{r\theta} = 0$$

where $D = 2\int_0^{\pi/2} (\cosh k\theta)^{1/n} \cos\theta \, d\theta$, and $k = n(n-2)$ for conditions of plane strain.† The stress field is a simple radial one as in the linear case. In that case $n = 1, k = \sqrt{(-1)}, (\cosh k\theta)^{1/n} = \cos\theta, D = \pi/2$ whereupon equation (6.75) reduces to equation (2.15). Note that the stress is zero at the free surface where $\theta = \pm\pi/2$. A special case arises when $n = 2; k = 0, D = 2$ and $\sigma_r = -P/2r$, which is independent of θ. With materials which strain-harden only to a moderate extent, $n > 2$, so that $k > 0$; the stress σ_r at constant radius r increases with θ from a minimum directly below the load ($\theta = 0$) to a maximum at the surface ($\theta = \pm\pi/2$). Expressions for the displacements $u_r(r, \theta)$ and $u_\theta(r, \theta)$ are given by Arutiunian (1959) for plane strain and by Venkatraman (1964) for plane stress.

The stresses, strains and displacements at any point in the solid are directly proportional to the applied load P; so also are increments of stress and strain acquired in a time increment dt. This implies that the above solution, derived

† The problem has been solved by Venkatraman (1964) for 'plane stress', for which $k = n(n-3)/2$.

Fig. 6.25. Nonlinear power-law material: $\epsilon = \epsilon_0(\sigma/\sigma_0)^n$. Linear elastic: $n = 1, E = \sigma_0/\epsilon_0$. Perfectly-plastic, $n = \infty$, $Y = \sigma_0$.

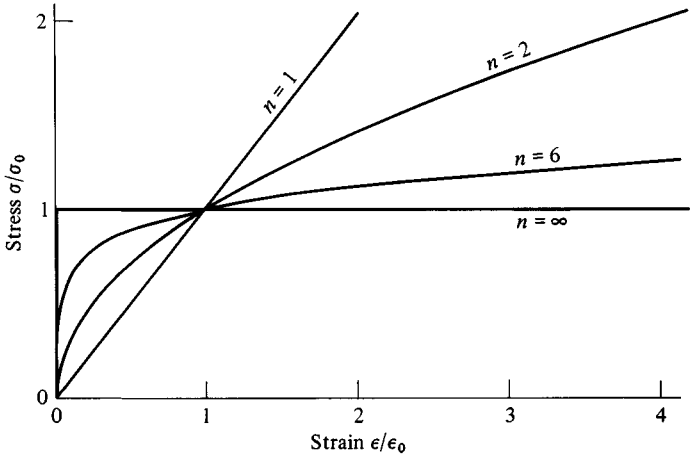

for a nonlinear elastic material specified by equation (6.73), applies equally to a creeping material specified by (6.74) in which strains are replaced by strain rates and displacements by velocities.

The stresses and displacements due to a point force acting on a nonlinear half-space - the nonlinear equivalent of the problem considered in §3.2 - have been analysed by Kuznetsov (1962).

Contact of nonlinear solids

For linear materials, whether elastic or viscoelastic, the stresses and displacements caused by a concentrated force can be superposed to find the stresses and displacements caused by a distributed load or by the contact of bodies with known profiles. With nonlinear materials the principle of superposition is no longer applicable, but Arutiunian (1959) argues that the surface displacement produced by a distributed load acting on a small segment of the boundary of a nonlinear half-space can be expressed by a series expansion whose dominant term is that obtained by the superposition of the displacements given by the solution for a concentrated force described above. On the basis of this approximation, expressions are developed from which the contact size and pressure distribution at any time can be found numerically when the value of the index n in equation (6.73) or (6.74) is specified.

In the special case of a rigid die with a flat base indenting a nonlinear half-space, the boundary conditions at the contact surface for a nonlinear elastic body (e.g. (6.73)) and a power law creeping solid (e.g. (6.74)) are analogous. In the first case the displacement $\bar{u}_z = \text{constant} = \delta$, and in the second the surface velocity $\dot{\bar{u}}_z = \text{constant} = \dot{\delta}$. The situation is similar, therefore, to loading by a concentrated force discussed above: the pressure on the face of the die is the same for both nonlinear elasticity and nonlinear creep. For a two-dimensional punch Arutiunian (1959) finds

$$p(x,t) = \frac{\Gamma\left(\frac{3n-1}{2n}\right)\Gamma\left(\frac{1}{2n}\right)\sin(\pi/2n)}{a\pi^{1/2}} \frac{P(t)}{\pi(1-x^2/a^2)^{1/2n}} \tag{6.76}$$

where Γ denotes a Gamma function, and for the axi-symmetric punch Kuznetsov (1962) shows that

$$p(r,t) = \frac{(2n-1)}{2\pi n a^2} \frac{P(t)}{(1-r^2/a^2)^{1/2n}} \tag{6.77}$$

For a linear elastic material, where $n = 1$, both expressions reduce as expected to the elastic pressure on the base of a rigid punch, i.e. to equations (2.64) and (3.34). In the other extreme of a perfectly plastic material, $n \to \infty$, and the contact pressures given by equations (6.76) and (6.77) become uniform. This

agrees exactly with the slip-line field solution for a two-dimensional punch in which the pressure is $2.97Y$, where Y is the yield stress in tension or compression. For a punch of circular plan-form the slip-line field solution gives a pressure which peaks slightly towards the centre of the punch (see Fig. 6.10), with an average value $p_m = 2.85Y$.

With an indenter whose profile is curved rather than flat the behaviour in steady creep is different from that of nonlinear elasticity because (*a*) the *displacements* imparted to the surface vary over the face of the indenter whereas the *velocity* of the indenter is uniform and (*b*) the contact area grows during the indentation so that material elements do not experience proportional loading. In these circumstances the analysis by Arutiunian's method becomes very involved while remaining approximate through the use of superposition. An alternative approximate treatment of the contact of spheres which is attractive by its simplicity has been suggested by Matthews (1980). We shall look first at a nonlinear material which deforms according to equation (6.73), as shown in Fig. 6.25. Guided by Kuznetsov's result for a rigid punch (eq. (6.77)), the pressure distribution is assumed to be given by:

$$p(r) = \frac{2n+1}{2n} p_m (1 - r^2/a^2)^{1/2n} \tag{6.78}$$

For a linear elastic incompressible material ($n = 1$) this distribution reduces to that of Hertz for which $p_m = 16Ea/9\pi R$ (eqs. (4.21), (4.22) and (4.24)). Putting $n = \infty$ in equation (6.78) gives a uniform pressure. For a perfectly plastic material the pressure distribution given by the slip-line field solution, shown in Fig. 6.10, is roughly uniform with $p_m \approx 3Y$. Both of these values of p_m, corresponding to the extreme values of n (1 and ∞), are realised if we write

$$\frac{P}{\pi a^2} = p_m = \frac{6n\sigma_0}{2n+1} \left(\frac{8a}{9\pi R \epsilon_0} \right)^{1/n} \tag{6.79}$$

since, in the constitutive equation (6.73), $\sigma_0/\epsilon_0{}^{1/n} = E$ when $n = 1$ and $\sigma_0 = Y$ when $n \to \infty$. It is reasonable to suppose that equation (6.79) then gives a good approximation to the relationship between load P and contact size a for intermediate values of n. In his study of hardness, Tabor (1951) suggested the empirical relationship

$$p_m \approx 3Y_R \tag{6.80}$$

where Y_R is the stress at a representative strain ϵ_R in a simple compression test. For a material with power law hardening, $Y_R = \sigma_0(\epsilon_R/\epsilon_0)^{1/n}$. Substituting for Y_R in (6.80) enables ϵ_R to be found from equation (6.79), thus:

$$\epsilon_R = \frac{8}{9\pi} \left(\frac{2n}{2n+1} \right)^n \frac{a}{R} \tag{6.81}$$

https://doi.org/10.1017/CBO9781139171731.007 Published online by Cambridge University Press

which varies from $0.188a/R$ to $0.171a/R$ as n varies from 1 to ∞. The variation with n is small and the values are reasonably consistent with Tabor's empirical result: $\epsilon_R \approx 0.2(a/R)$, independent of the precise shape of the stress-strain curve.

The penetration δ of the indenter into the half-space is of interest. Based on the experimental data of Norbury & Samnuel (1928) Matthews proposes the expression:

$$\delta = \left(\frac{2n}{2n+1}\right)^{2(n-1)} \frac{a^2}{R} \tag{6.82}$$

Thus δ varies from the elastic value a^2/R when $n = 1$ to $0.368a^2/R$ when $n = \infty$, which is in good agreement with the perfectly plastic analysis of Richmond *et al.* (1974). When $\delta > a^2/2R$ the periphery of the indentation 'sinks in' below the surface of the solid, as described in §3. This occurs for low values of n, i.e. with annealed materials. When n exceeds 3.8, $\delta < a^2/2R$ and 'piling up' occurs outside the edge of the contact.

We turn now to penetration by a spherical indenter under conditions of power law creep governed by equation (6.74). Matthews assumes that the pressure distribution is the same as that found by Kuznetsov for a flat-faced punch (eq. (6.77)), i.e.

$$p(r,t) = \frac{2n-1}{2n} p_m(t)(1 - r^2/a^2)^{-1/2n} \tag{6.83}$$

For $n = 1$, equation (6.74) describes a linear viscous material of viscosity $\eta = \sigma_0/3\dot{\epsilon}_0 = 1/3B$. Spherical indentation of such a material was analysed in §5, where it was shown (eq. (6.67)) that

$$p(r,t) = \frac{8\eta\dot{a}}{\pi R}(1 - r^2/a^2)^{-1/2} \tag{6.84}$$

By differentiating equation (6.66) with respect to time we get

$$p_m(t) = \frac{P(t)}{\pi a^2} = \frac{16\eta}{\pi R}\dot{a} = \frac{8\eta\dot{\delta}}{\pi(R\delta)^{1/2}} \tag{6.85}$$

For $n \to \infty$, the nonlinear viscous material also behaves like a perfectly plastic solid of yield stress $Y = \sigma_0$, so that $p_m \approx 3Y$.

If, for the nonlinear material, we now write

$$p_m(t) = \frac{P(t)}{\pi a^2} = \frac{6n\sigma_0}{2n-1}\left(\frac{8\dot{a}}{9\pi R\dot{\epsilon}_0}\right)^{1/n} \tag{6.86}$$

Equations (6.83) and (6.86) reduce to (6.84) and (6.85) when $n = 1$ and $\sigma_0/3\dot{\epsilon}_0 = \eta$, and reduce to $p_m = \text{constant} = 3Y$ when $n = \infty$. Making use of the

https://doi.org/10.1017/CBO9781139171731.007 Published online by Cambridge University Press

relationship (6.82) the velocity of penetration $\dot{\delta}$ can be written

$$\dot{\delta}(t) = 2(\delta/R)^{1/2} \left(\frac{2n}{2n+1} \right)^{n-1} \dot{a}(t) \tag{6.87}$$

where $\dot{a}$ is related to the load by equation (6.86). In a given situation either the load history $P(t)$ or the penetration history $\delta(t)$ would be specified, whereupon equations (6.86) and (6.83) enable the variations in contact size $a(t)$ and contact pressure $p(r, t)$ to be found if the material parameters σ_0, $\dot{\epsilon}_0$ and n are known.

https://doi.org/10.1017/CBO9781139171731.007 Published online by Cambridge University Press